IEEE Access
Multidisciplinary ⋮ Rapid Review ⋮ Open Access Journal

Received 25 July 2024, accepted 1 August 2024, date of publication 5 August 2024, date of current version 16 August 2024.

Digital Object Identifier 10.1109/ACCESS.2024.3438753

RESEARCH ARTICLE

Research on an Improved Wasserstein Generative Adversarial Network Early Fault Warning Method for Rotating Machinery

CHUNLEI ZHOU[1,3], WANG XIAO[2], QINGFENG WANG[1], (Member, IEEE), AND ZHIPENG FENG[3], (Member, IEEE)

[1]State Key Laboratory of High-End Compressor and System Technology, Beijing University of Chemical Technology, Beijing 100029, China
[2]Western Branch of National Pipe Network Group United Pipeline Company Ltd., Ürümqi 830013, China
[3]School of Mechanical Engineering, University of Science and Technology Beijing, Beijing 100083, China

Corresponding author: Qingfeng Wang (wangqf2422@buct.edu.cn)

This work was supported in part by the National Key Research and Development Program of China under Grant 2023YFF0612701 and Grant 2023YFC3010504, and in part by the Major Projects of PipeChina under Grant WZXGL202107.

ABSTRACT Early fault warning for large-scale high-speed rotating machinery can effectively reduce unplanned downtime and avoid major safety accidents. Aiming at the problems of difficult screening of multi-source common sensitive features, the challenging training of neural networks with a small number of sensitive features, and the difficulty of directly using generative adversarial networks for early fault warning, this paper constructs an early fault warning model based on multi-source common sensitive features and an improved Wasserstein generative adversarial network, proposing an early fault warning method for rotating machinery. The model was verified by using the open XJTU-SY bearing laboratory data, the P3409A centrifugal pump bearing fault engineering case data of a petrochemical company and the rotor system engineering case data of a circulating hydrogen centrifugal compressor of a petrochemical company. The early fault warning method of rotating machinery proposed in this paper warns the bearing fault of centrifugal pump 160 hours in advance and the rotor system fault of centrifugal compressor 1330 minutes in advance. Compared with the two published methods, the proposed method has better early fault warning effect, better normal and abnormal health index discrimination and less false warning.

INDEX TERMS Rotating machines, deep learning, generative adversarial networks, early fault warning.

I. INTRODUCTION

High-speed rotating machinery is extensively utilized in petrochemical industries on a large scale. To meet the economic demands of industrial safety production, maintaining the equipment's long-term stable performance is essential. Once the unplanned shutdown of the equipment occurs, it will lead to production interruption and even serious safety accidents, resulting in significant economic losses. Early fault warning is designed to provide timely and precise alerts at the initial emergence or when the severity of a fault in equipment is still low. This enables the guidance of equipment operation and maintenance, monitoring of fault progression, effective containment of fault escalation, and assurance of the equipment's safe, stable, and reliable performance [1]. However, early fault symptoms in rotating machinery are often weak, with indistinct characteristics, and they operate in complex environments where fault signals can be easily obscured by noise. This presents challenges for early fault warning. Common early fault warning methods are based on traditional time-frequency signal analysis and processing methods, traditional machine learning model methods, and deep learning model methods.

The early fault warning method based on traditional time-frequency signal analysis and processing relies on smooth filtering, decomposition, and noise reduction of the original signal. Subsequently, the time-frequency features are extracted from the original signal, and the features of

The associate editor coordinating the review of this manuscript and approving it for publication was Jiachen Yang.

© 2024 The Authors. This work is licensed under a Creative Commons Attribution-NonCommercial-NoDerivatives 4.0 License.
For more information, see https://creativecommons.org/licenses/by-nc-nd/4.0/

the real-time signal are compared with the calculated fault features to identify the early fault. Tian et al. [2] studied an early warning method for rolling bearing faults utilizing beta distribution and a noise filtering reduction algorithm. They employed the XJTU-SY dataset along with experimental bearing data to validate the algorithm's precision. Guo et al. [3] proposed an improved version of symplectic geometry mode decomposition for rotating machinery faults detection and confirmed its effectiveness with numerical and experimental investigations. Wang et al. [4] proposed an early fault warning method utilizing a multi-scale enhanced morphological top-hat filter based on adaptive variational mode decomposition-sample entropy noise reduction. The method demonstrated superior diagnostic capabilities for detecting weak faults amidst noise interference, as evidenced by both experimental and engineering outcomes. Xu and Li [5] proposed a novel empirical variational mode decomposition and exact Teager energy operator for early fault detection of rotating machinery and confirmed its effectiveness with simulation data and experimental data. These methods have strong interpretability, but they have the following shortcomings: (1) The need to manually establish standards and thresholds frequently compromises the adaptability of these methods. (2) Noise reduction is often necessary. However, while it eliminates interference, it can also diminish the early signs of faults.

The early fault warning method based on the traditional machine learning model extracts the spectral features [6], wavelet features [7], time-frequency features [8], entropy features [9], etc. of the condition monitoring signal, and then trains the machine learning model based on the extracted features to construct the alarm threshold line to achieve early fault warning. Shi et al. [10] introduced a novel early fault warning approach utilizing density clustering and the extreme gradient boosting algorithm, which was validated using data from wind turbines. Xiao et al. [11] proposed a method for early warning and diagnosis of sudden imbalance faults in rotating machinery. The method's effectiveness was confirmed through the application of real-world engineering fault cases from petrochemical companies as test data. Wang et al. [12] researched a data-driven model for early fault detection in rotating machinery. Utilizing wavelet packet decomposition and dynamic kernel principal component analysis among other techniques, they developed an early warning model. This method was validated using both public datasets and real-world engineering fault data. Kang et al. [13] employed a self-supervised deep one-class classification approach, trained exclusively with normal class samples, for the early detection of faults in rolling bearings. The efficacy of this method was confirmed through the application of two distinct sets of actual rolling bearing fault data. Wang et al. [14] introduced a method for early fault detection that combines improved L1 Trend Filtering with Support Vector Data Description (L1TF-SVDD). This approach has been validated using public bearing datasets and engineering datasets. The above methods are based on the normal equipment data, but there are still some shortcomings in the practical industrial application: (1) Characterizing fault features under complex operating conditions is challenging when only individual feature modeling is employed; (2) While traditional machine learning techniques like support vector machines and autoencoders are prevalent, they fall short in extracting deeper features that require more sophisticated architectures.

The method of early fault warning utilizing deep learning models has garnered significant interest among researchers in the domain of early fault warning, owing to the powerful feature learning capabilities of neural networks. Liu et al. [15] proposed a method for early fault warning in nuclear steam turbines using a Bayesian long short-term memory neural network. The experimental findings indicate that this approach can deliver precise early warnings during the initial phase of fault development. Gao et al. [16] proposed a method for early fault warning that utilizes an enhanced long short-term memory network combined with ensemble empirical mode decomposition energy moment entropy. This method was validated using publicly available bearing datasets. Peng et al. [17] proposed a MixMatch-based adversarial domain adaptive network for early fault warning of permanent magnet synchronous motors under various operating conditions. The method was tested and verified by four kinds of early fault data in permanent magnet synchronous motors under various operating conditions. Ding et al. [18] introduced a self-supervised pre-training based early fault warning method for rolling bearings, which was validated through the application of data from two different bearing test benches. Since the Generative Adversarial Network (GAN) was proposed, it has attracted extensive attention from researchers in many fields. GAN has a wide range of research in the field of fault diagnosis, but less research in the field of fault warning. Xu et al. [19] proposed an anomaly detection model based on AutoEncoder and Generative Adversarial Network (AE-GAN), which is applied to the early fault warning of high-speed trains.

However, the early fault warning method based on deep learning model also has some difficulties. Aiming at the problems that it is difficult to screen multi-source common sensitive features, the number of sensitive features is small, the neural network training is difficult, and the generative adversarial network is difficult to be directly used for early fault warning, this paper constructs an early fault warning model based on Multi-source Common Sensitive Features and Improved Wasserstein Generative Adversarial Network (MCSF-IWGAN-GP), and proposes an early fault warning method for rotating machinery. Additionally, this method overcomes the shortcomings of traditional time-frequency signal analysis and processing methods as well as traditional machine learning model methods. The contributions of this paper are as follows:

(1) A multi-source common sensitive feature screening method based on variance analysis F test is proposed, which

can automatically screen out early fault sensitive features with good generalization.

(2) An improved Wasserstein generative adversarial network is proposed. An input adaptive layer is added before the two-dimensional convolutional layer of the discriminator, so that it can adapt to input data of different lengths, and map low-dimensional features to high dimensions for neural network learning. The training function of WGAN-GP is improved to have the ability to discriminate ' normal ' or ' abnormal ' input data.

(3) An early fault early warning method for rotating machinery based on MCSF-IWGAN-GP is proposed. This method only needs the historical normal data of the equipment to be tested, and does not depend on expert experience or prior knowledge to achieve intelligent early warning of equipment faults.

The structure of this paper is organized in the following manner: Section II presents the empirical wavelet transform, Wasserstein generative adversarial network, and input adaptive layer. Section III details the proposed method. Section IV validates the proposed method using open laboratory data and engineering case data. Section V conducts a comparison of the proposed method with two existing published methods. Section VI concludes with a summary of findings and outlines directions for future work.

II. BASIC THEORIES

A. EMPIRICAL WAVELET TRANSFORM

Empirical Wavelet Transform (EWT), a novel method for adaptive wavelet construction, was introduced by Gilles [20]. It utilizes the fast Fourier transform to acquire the spectrum of the fault signal. According to the Shannon criterion, the spectrum is within $[0, \pi]$. The spectrum is divided into N segments, and ω_n is its boundary, that is $\omega_0 = 0$ and $\omega_N = \pi$. Then each frequency band is $\Lambda_n = [\omega_{n-1}, \omega_n]$, so $\bigcup_{n=1}^{N} \Lambda_n = [0, \pi]$ [21], [22]. The scaling function $\phi_n(\omega)$ and wavelet function $\psi_n(\omega)$ of empirical wavelets are as follows [23]:

$$\phi_n(\omega) = \begin{cases} 1, \text{if } |\omega| \le (1-\gamma)\omega_n \\ \cos\left[\frac{\pi}{2}\beta\left(\frac{1}{2\gamma\omega_n}(|\omega| - (1-\gamma)\omega_n)\right)\right], \\ \text{if } (1-\gamma)\omega_n \le |\omega| \le (1+\gamma)\omega_n \\ 0, \text{otherwise} \end{cases} \tag{1}$$

$$\psi_n\omega = \begin{cases} 1, \text{if } (1+\gamma)\omega_n \le |\omega| \le (1-\gamma)\omega_{n+1} \\ \cos\left[\frac{\pi}{2}\beta\left(\frac{1}{2\gamma\omega_{n+1}}(|\omega| - (1-\gamma)\omega_{n+1})\right)\right], \\ \text{if } (1-\gamma)\omega_{n+1} \le |\omega| \le (1+\gamma)\omega_{n+1} \\ \sin\left[\frac{\pi}{2}\beta\left(\frac{1}{2\gamma\omega_n}(|\omega| - (1-\gamma)\omega_n)\right)\right], \\ \text{if } (1-\gamma)\omega_n \le |\omega| \le (1+\gamma)\omega_n \\ 0, \text{otherwise} \end{cases} \tag{2}$$

where $\beta(x) = x^4\left(35 - 84x + 70x^2 - 20x^3\right)$, $\tau_n = \gamma\omega_n$, $0 < \gamma < 1$.

The detail coefficient $W_f^{\varepsilon}(n, t)$ and approximation coefficient $W_f^{\varepsilon}(0, t)$ of empirical wavelet transform are as follows:

$$W_f^{\varepsilon}(n, t) = \langle f, \psi_n \rangle = \int f(\tau)\,\overline{\psi_n(\tau - t)}d\tau = \left(\hat{f}(\omega)\,\overline{\hat{\psi}_n(\omega)}\right)^{\vee} \tag{3}$$

$$W_f^{\varepsilon}(0, t) = \langle f, \phi_1 \rangle = \int f(\tau)\,\overline{\phi_1(\tau - t)}d\tau = \left(\hat{f}(\omega)\,\overline{\hat{\phi}_1(\omega)}\right)^{\vee} \tag{4}$$

Therefore, the original signal is reconstructed as:

$$f(t) = W_f^{\varepsilon}(0, t) * \phi_1(t) + \sum_{n=1}^{N} W_f^{\varepsilon}(n, t) * \psi_n(t) = \left(\hat{W}_f^{\varepsilon}(0, \omega) * \hat{\phi}_1(\omega) + \sum_{n=1}^{N} \hat{W}_f^{\varepsilon}(n, \omega) * \hat{\psi}_1(\omega)\right)^{\vee} \tag{5}$$

where $\hat{}$ is the Fourier transform, $\check{}$ is the inverse Fourier transform, $\bar{}$ is the complex conjugate, and $*$ is the convolution.

B. WASSERSTEIN GENERATIVE ADVERSARIAL NETWORK WITH GRADIENT PENALTY

Generative Adversarial Network (GAN) [24] is a powerful generative model, which is composed of generator G and discriminator D. The two compete with each other through a game theory framework, and then get optimized. The structure of GAN is shown in Fig.1. Although traditional GAN can generate high-quality samples, it faces problems such as instability and mode collapse during training. In order to solve these problems, Arjovsky et al. [25] proposed WGAN, which introduces Wasserstein distance as a method to stabilize the training process. On this basis, Gulrajani et al. [26] proposed WGAN-GP, which further introduced gradient penalty to ensure the Lipschitz continuity of the discriminator, thus improving the training stability and sample diversity.

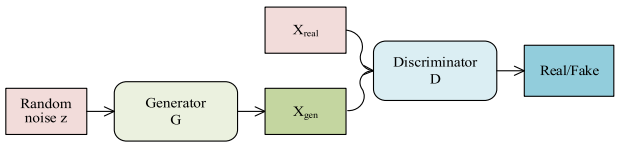

FIGURE 1. Architecture of GAN.

WGAN-GP uses Wasserstein distance instead of Jensen-Shannon divergence in traditional GAN. The Wasserstein distance provides an effective way to quantify the difference between the generated data distribution and the real data distribution. Compared with the Jensen-Shannon divergence, the Wasserstein distance can provide a more continuous gradient, even when there is no overlap between distributions, which helps to improve the stability and convergence of GAN training. In addition, in order to force the discriminator to satisfy the Lipschitz constraint, WGAN-GP introduces a gradient penalty. This technique imposes constraints on the

gradients of the random interpolation between the real sample and the generated sample by the discriminator to ensure that the norm of these gradients does not exceed a predetermined constant. This penalty is achieved by adding a regular term to the discriminator loss function, which penalizes the behavior of the gradient norm deviating from 1.

The training of WGAN-GP involves a max-min game, where the discriminator aims to maximize the following loss function:

$$L_D = E_{Z\sim P_Z}\left[D\left(G\left(z\right)\right)\right] - E_{X\sim P_{data}}\left[D\left(x\right)\right] + \lambda E_{\hat{X}\sim P_{\hat{X}}}\left[\left(\left\|\nabla_{\hat{X}} D\left(\hat{x}\right)\right\|_2 - 1\right)^2\right] \tag{6}$$

where $D(x)$ is the output of the discriminator, x is the sample from the real data distribution P_{data}, and $G(z)$ is the sample generated by the generator from the data distribution P_Z. $\hat{x}$ is the interpolation between the real sample and the generated sample, which is used to calculate the gradient penalty. λ is the weight of gradient penalty.

The generator's goal is to minimize its own losses:

$$L_G = -E_{Z\sim P_Z}\left[D\left(G\left(z\right)\right)\right] \tag{7}$$

The maximum and minimum objective function of WGAN-GP is:

$$\min_G \max_D E_{X\sim P_{data}}\left[D\left(x\right)\right] - E_{Z\sim P_Z}\left[D\left(G\left(z\right)\right)\right] - \lambda E_{\hat{X}\sim P_{\hat{X}}}\left[\left(\left\|\nabla_{\hat{X}} D\left(\hat{x}\right)\right\|_2 - 1\right)^2\right] \tag{8}$$

C. INPUT ADAPTIVE LAYER

In comparison to one-dimensional CNNs, two-dimensional CNNs exhibit superior capabilities in feature extraction and classification [28]. In the field of fault diagnosis, many scholars use two-dimensional convolution structure to construct neural network model [29], [30], [31]. Consequently, the generative adversarial network proposed in this study incorporates a two-dimensional convolutional structure. Nonetheless, the vibration signals from rotating machinery are one-dimensional and often cannot be directly transformed into two-dimensional data for convolutional operations. Furthermore, the data volume diminishes after the initial vibration signal undergoes feature extraction and sensitive feature selection. Zhou et al. [32] developed an input adaptive layer capable of converting one-dimensional data of any length into two-dimensional data suitable for convolutional operations. This layer also enables the mapping of low-dimensional features to higher dimensions, facilitating neural network learning and accommodating varying lengths of input data.

The one-dimensional signal with length m is defined as:

$$S_{input} = \left[a_1\ a_2\ \cdots\ a_m\right] \tag{9}$$

where S_{input} represents one-dimensional input data, and a_i represents the value of node i of one-dimensional waveform data.

To transform one-dimensional data of non-square length m into two-dimensional data of the desired size, an input vector S_{input} of size $(1,m)$ is multiplied by a weight matrix of size (m, n). This process converts the input data into a one-dimensional vector of square length n, after which the results are adjusted as demonstrated in (10).

$$S = F_A\left(S_{input}\cdot K + b\right) \tag{10}$$

where K represents the weight matrix formulated by the kernel layer, as indicated in (11); b denotes the bias vector produced by the bias layer, as referenced in (12); $\mathrm{F_A}(\cdot)$ is the activation function utilized within the neural network.

$$K = \begin{bmatrix} k_{11} & k_{12} & \cdots & k_{1n} \\ k_{21} & k_{22} & \cdots & k_{2n} \\ \vdots & \vdots & \ddots & \vdots \\ k_{m1} & k_{m2} & \cdots & k_{mn} \end{bmatrix} \tag{11}$$

$$b = \begin{bmatrix} b_1\ b_2\ \cdots\ b_n \end{bmatrix} \tag{12}$$

By substituting (11) and (12) into (10), the transformed value of the i-th node can be determined as follows:

$$S_i = F_A\left(\sum_{j=1}^{m} a_j \times k_{ji} + b_i\right) \tag{13}$$

Given that n is a perfect square, it simplifies the transformation of one-dimensional data with length $(1,n)$ into a two-dimensional array with dimensions $(\sqrt{n}, \sqrt{n})$.

$$S_{output} = F_R\left(S\right) \tag{14}$$

where $\mathrm{F_R}(\cdot)$ denotes Reshape function.

Equations (9) through (14) detail the derivation process of IAL. IAL is defined in the following manner:

$$S_{2D} = IA\left(S_{1D}\right) \tag{15}$$

where $\mathrm{IA}(\cdot)$ denotes the input adaptive function that takes one-dimensional data of any length and outputs two-dimensional data of the specified size.

When the length of one-dimensional data is small, the expected size of two-dimensional data can be set to a larger square by inputting the adaptive layer, and this process enables the mapping of low-dimensional features to a higher-dimensional space, facilitating the feature learning process for neural networks.

III. PROPOSED METHOD

A. CONSTRUCTION OF MCSF-IWGAN-GP MODEL

The structure of the early warning model based on multi-source common sensitive features and IWGAN-GP is shown in Fig.2. The model consists of three parts: multi-scale mixed feature extraction of rotating machinery vibration signals, early fault sensitive feature screening of multi-source data, and early warning of IWGAN-GP. Firstly, the original vibration signals of rotating machinery collected by sensors, such as bearing signals, rotor system signals, etc., are decomposed by empirical wavelet transform to obtain the three order IMF components of the original signal. The time domain features, frequency domain features and time-frequency features

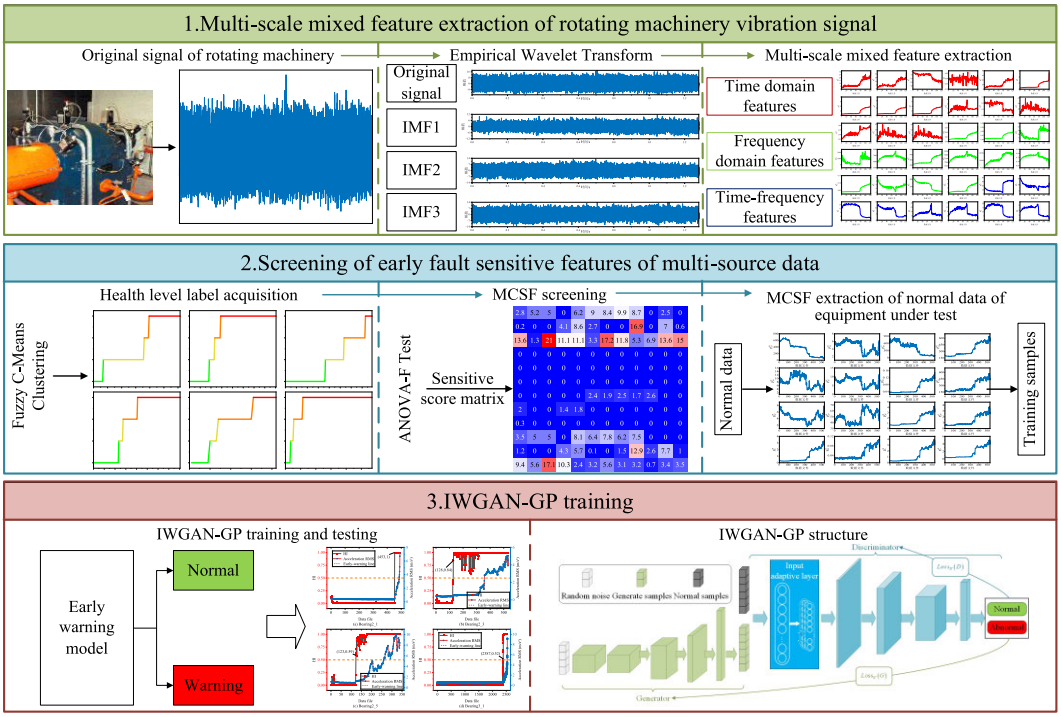

FIGURE 2. Structure diagram of early warning model based on MCSF-IWGAN-GP.

of the original signal and the three order IMF components are extracted respectively, and the multi-scale mixed features are obtained. Then, the Fuzzy C-means clustering (FCM) is used to obtain the health level label of multi-source data, which is used as the category label, and the sensitive feature screening based on the Analysis of Variance F test (ANOVA-F) is used. Then, the sensitive features selected from the normal data of the equipment to be tested are extracted as training samples. Finally, IWGAN-GP is trained for early warning using normal samples of the equipment to be tested.

1) MULTI-SCALE MIXED FEATURE EXTRACTION

Upon the failure of specific equipment, concurrent alterations occur in associated signal characteristics. These include changes in amplitude and probability distribution within the time domain, variations in energy across different frequencies in the frequency domain, shifts in the primary energy spectrum's leading edge, and modifications in the time-frequency power's structural distribution. When a potential fault occurs in a rotating machinery, extracting early faults sensitive features is the key to early fault warning. To screen features that are indicative of early faults and possess generalizability, it is essential to initially perform feature extraction in the time domain, frequency domain, and time-frequency domain from multi-source data. Under complex working conditions, decomposing the vibration signal to create multi-scale mixed features provides a more comprehensive representation of the health status of rotating machinery. This study introduces a multi-scale mixed feature extraction approach for the vibration signals of rotating machinery. The method involves decomposing the original vibration signal using EWT, followed by extracting multi-scale mixed features of the time domain, frequency domain, and time-frequency domain from both the original signal and its Intrinsic Mode Functions (IMF).

The vibration signal is decomposed by empirical wavelet transform to obtain the three order IMF components IMF1, IMF2 and IMF3 of the original signal. For the original signal and the three order IMF components, 15 time-domain features $p_1 - p_{15}$, 13 frequency-domain features $p_{16} - p_{28}$ and 8 time-frequency features $p_{29} - p_{36}$ are extracted respectively. The time domain features $p_1 - p_{15}$ are shown in TABLE 1, the frequency domain features $p_{16} - p_{28}$ are shown in TABLE 2, and the time-frequency features $p_{29} - p_{36}$ are analyzed by three-layer wavelet packet analysis of the vibration signal. The energy percentage of the eight sub-bands in the last layer is used as the time-frequency feature.

Let a signal time domain sequence $x(n)$, $n = 1, 2, \cdots, N$, N be the number of sample points, then the above 15 time domain characteristic parameters are defined as shown in Table 1.

Let $s(k)$ be the frequency spectrum of the signal $x(n)$, $k = 1, 2, \cdots, K$, K be the number of spectral lines, f_k be the frequency value of the kth spectral line, and 13 frequency domain characteristic parameters are defined as shown in Table 2.

The multi-scale mixing features of the original signal are denoted as $p_1^0 - p_{36}^0$, the multi-scale mixing relative features of the first-order IMF component are denoted as $p_1^1 - p_{36}^1$, the multi-scale mixing relative features of the second-order

TABLE 1. feature parameter in Time domain.

Parametric Expression	Parametric Expression
$p_1 = \max(x_n)$	$p_9 = \sqrt{\frac{1}{N-1}\sum_{n=1}^{N}\left[x(n)-\bar{x}\right]^2}$
$p_2 = \max(\lvert x_n\rvert)$	$p_{10} = \frac{\sum_{n=1}^{N}\left[x(n)-\bar{x}\right]^4}{(N-1)\sigma^4}$
$p_3 = \min(x_n)$	$p_{11} = \frac{\sum_{n=1}^{N}\left[x(n)-\bar{x}\right]^3}{(N-1)\sigma^3}$
$p_4 = \frac{1}{N}\sum_{n=1}^{N}x(n)$	$p_{12} = \frac{\max\lvert x(n)\rvert}{x_{\mathrm{rms}}}$
$p_5 = x_{\max} - x_{\min}$	$p_{13} = \frac{x_{\mathrm{rms}}}{\bar{x}}$
$p_6 = \frac{1}{N}\sum_{n=1}^{N}\lvert x_n\rvert$	$p_{14} = \frac{\max\lvert x(n)\rvert}{\bar{x}}$
$p_7 = \sqrt{\frac{1}{N}\sum_{n=1}^{N}x^2(n)}$	$p_{15} = \frac{\max\lvert x(n)\rvert}{x_r}$
$p_8 = \left(\frac{1}{N}\sum_{n=1}^{N}\sqrt{\lvert x(n)\rvert}\right)^2$	

TABLE 2. feature parameter in frequency domain.

Parametric Expression	Parametric Expression
$p_{16} = \frac{\sum_{k=1}^{K}s(k)}{K}$	$p_{23} = \sqrt{\frac{\sum_{k=1}^{K}f_k^4 s(k)}{\sum_{k=1}^{K}f_k^2 s(k)}}$
$p_{17} = \frac{\sum_{k=1}^{K}\left(s(k)-p_{16}\right)^2}{K-1}$	$p_{24} = \frac{\sum_{k=1}^{K}f_k^2 s(k)}{\sqrt{\sum_{k=1}^{K}s(k)\sum_{k=1}^{K}f_k^4 s(k)}}$
$p_{18} = \frac{\sum_{k=1}^{K}\left(s(k)-p_{16}\right)^3}{K\left(\sqrt{p_{17}}\right)^3}$	$p_{25} = \frac{p_{21}}{p_{20}}$
$p_{19} = \frac{\sum_{k=1}^{K}\left(s(k)-p_{16}\right)^4}{Kp_{17}^2}$	$p_{26} = \frac{\sum_{k=1}^{K}\left(f_k-p_{20}\right)^3 s(k)}{Kp_{21}^3}$
$p_{20} = \frac{\sum_{k=1}^{K}f_k s(k)}{\sum_{k=1}^{K}s(k)}$	$p_{27} = \frac{\sum_{k=1}^{K}\left(f_k-p_{20}\right)^4 s(k)}{Kp_{21}^4}$
$p_{21} = \sqrt{\frac{\sum_{k=1}^{K}\left(f_k-p_{20}\right)^2 s(k)}{K}}$	$p_{28} = \frac{\sum_{k=1}^{K}\left(f_k-p_{20}\right)^{1/2} s(k)}{K\sqrt{p_{21}}}$
$p_{22} = \sqrt{\frac{\sum_{k=1}^{K}f_k^2 s(k)}{\sum_{k=1}^{K}s(k)}}$	

IMF component are denoted as $p_1^2 - p_{36}^2$, and the multi-scale mixing relative features of the third-order IMF component are denoted as $p_1^3 - p_{36}^3$, totaling $(15 + 13 + 8) \times 4 = 144$ multi-scale mixing features.

2) MULTI-SOURCE COMMON SENSITIVE FEATURE SCREENING

Different features have different sensitivity to the early fault of different data. Based on the sensitive features of multi-source data, the common sensitive features are screened out. This process strengthens the generalization capability of sensitive features, thereby enhancing the performance of early fault warning models. In order to screen out the common sensitive features with good generalization for early faults, this paper proposes a multi-source common sensitive feature screening method based on ANOVA-F test. Analysis of Variance F test [27] is a statistical method for feature selection, which is based on ANOVA to assess whether there are significant differences in the mean values between different groups. In machine learning, ANOVA is especially used to determine whether the relationship between each feature and the response variable is statistically significant, thereby helping to select the features most relevant to the prediction task. The sensitive features required for early warning need significant differences between the normal state and the fault state, so ANOVA can be used to screen for these sensitive features.

Firstly, FCM is applied to obtain health level label of multi-source data as the response variable of ANOVA. According to the health level label, each feature is divided into several groups, and the same health level is classified into one group.

According to the grouping of health levels, the F statistic is calculated:

$$F = \frac{\sum_{i=1}^{k} n_i \left(\overline{x_i} - \overline{x}\right)^2 / (k-1)}{\sum_{i=1}^{k}\sum_{j=1}^{n_i}\left(x_{ij} - \overline{x_i}\right)^2 / (N-k)} \tag{16}$$

where k represents the number of groups, which is the health grade. Generally, the whole life data of rotating machinery is divided into four levels. n_i represents the number of eigenvalues in group i, $\bar{x}_i$ is the average value of eigenvalues in group i, $\bar{x}$ is the average value of all eigenvalues of the feature, and N is the total number of eigenvalues.

Then, the F statistics of 144 multi-scale mixed features are calculated, and the first 36 features with the largest F statistics are recorded as follows:

$$P_{F\,i} = \begin{bmatrix} p_{F1} & \cdots & p_{F6} \\ \vdots & \ddots & \vdots \\ p_{F31} & \cdots & p_{F36} \end{bmatrix} \tag{17}$$

The ranking of the selected features represents their degree of sensitivity to early faults, so the top-ranked F statistic is given a high weight value. The ranking weight matrix is defined as:

$$K_{score\,i} = \begin{bmatrix} w_1 & \cdots & w_6 \\ \vdots & \ddots & \vdots \\ w_{31} & \cdots & w_{36} \end{bmatrix} \tag{18}$$

Due to the different personality features of different data, the sensitive features selected will be different. In order to screen out the features with good generalization, ANOVA F test is performed on the multi-source data, and the selected features are assigned weight values according to the ranking.

The sensitive feature weight values of multi-source data are superimposed to calculate the sensitive score matrix:

$$S = \sum \text{SSCFunction}(P_{F\,i},\ K_{score\,i}) = \begin{bmatrix} s_1 & s_2 & \cdots & s_{12} \\ s_{13} & s_{14} & \cdots & s_{24} \\ \vdots & \vdots & \vdots & \vdots \\ s_i & s_{i+1} & \cdots & s_{i+12} \\ \vdots & \vdots & \vdots & \vdots \\ s_{133} & s_{134} & \cdots & s_{144} \end{bmatrix} \tag{19}$$

where SSCFunction(·) is the formula for calculating the sensitive score, and s_i represents the sensitive score of the ith feature among the 144 features.

Finally, the first 16 features with the largest sensitivity scores are taken as multi-source common sensitive features.

3) IWGAN-GP

The discriminator of WGAN-GP can discriminate true or false samples. In the training function, the true sample is labeled as 1, and the false sample is labeled as 0. In order to use WGAN-GP for early fault warning, its training function and discriminator structure are improved to enable it to distinguish between normal and abnormal.

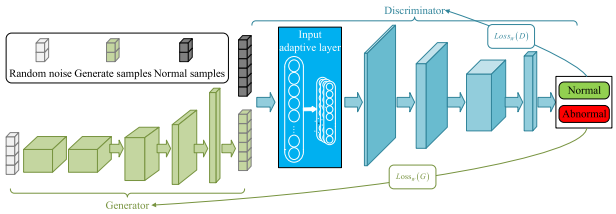

FIGURE 3. Structure diagram of IWGAN-GP.

The improved WGAN-GP structure diagram is shown in Fig.3. The training sample of IWGAN-GP is only the normal sample of the equipment to be tested. In the training function, the training sample (normal sample) is defined as 0, and the sample generated by the generator is 1. During model training, if the generator's performance is suboptimal, it results in low-quality samples that do not match the data distribution of the training set. Therefore, the discriminator will discriminate it as 1, which is opposite to the normal definition and is defined as abnormal. As training optimization advances, both the discriminator and generator improve in performance, leading to a steady enhancement in the quality of generated samples which increasingly resemble the training data distribution. In this process, the discriminator becomes increasingly accurate in identifying normal samples. The discriminator's final layer employs a Sigmoid activation function, producing an output value ranging between 0 and 1.

During the training of the original WGAN-GP, the adversarial process optimizes both the generator and the discriminator, eventually reaching a Nash equilibrium. At this point, the discriminator is unable to distinguish real samples from generated ones, resulting in an output value of 0.5. Therefore, when IWGAN-GP is used for early fault warning, the alarm threshold line is defined as 0.5. If the discriminator's output falls within the range of [0, 0.5), the input is classified as a normal sample. Conversely, if the output lies within the range of [0.5, 1], the input is classified as an abnormal sample.

Fig.3 illustrates the addition of an input adaptive layer prior to the first convolutional layer in the discriminator. According to the definition of the multi-source common sensitive feature screening part, the number of sensitive features screened is only 16. Training neural networks requires a substantial amount of data, so insufficient data can hinder the effectiveness of the model training process. The input adaptive layer is capable of transforming one-dimensional data into two-dimensional data, and it can also elevate low-dimensional features to higher dimensions during this process, thereby facilitating the neural network model's ability to learn the characteristics of the input data more effectively. In Equation (11), where n is a number exceeding 16, the low-dimensional feature data, initially with an input length of 16, can be transformed into high-dimensional feature data of length n. This approach addresses the challenge of having a limited number of sensitive features and the neural network training is difficult.

B. EARLY FAULT WARNING METHOD BASED ON MULTI-SOURCE COMMON SENSITIVE FEATURES AND IWGAN-GP

In this paper, an early fault warning method for rotating machinery based on MCSF-IWGAN-GP is proposed. The early fault warning model architecture of off-line training and on-line monitoring is adopted. The method flow is shown in Fig.4. The specific steps are as follows:

Step 1: The empirical wavelet transform is used to decompose the multi-source data D_M and extract the multi-scale mixed feature F_{MSM};

Step 2: Use FCM to obtain the health level label L of multi-source data;

Step 3: The feature screening method based on variance analysis F test is used to screen multi-source common sensitive features, and the index $Index_{FC}$ of common sensitive features in 144 multi-scale mixed features is obtained;

Step 4: After the normal data D_N of the equipment to be tested is decomposed by empirical wavelet transform, the common sensitive feature F_{CN} obtained by step 3 is extracted;

Step 5: The common sensitive feature F_{CN} of the normal data of the equipment to be tested is used as the training data, and the IWGAN-GP is trained as the early warning model;

Step 6: The real-time data D_T of the equipment to be tested is decomposed by empirical wavelet transform;

Step 7: Extract the common sensitive feature F_{CT} obtained by step 3;

Step 8: The common sensitive features of the real-time data of the equipment to be tested are input into the early warning model obtained by step 5, and the early fault warning result R_{EW} can be obtained.

In the above steps, steps 1-5 are offline training mode, steps 6-8 are online monitoring mode, and the pseudo code of early fault warning method is shown in Algorithm1.

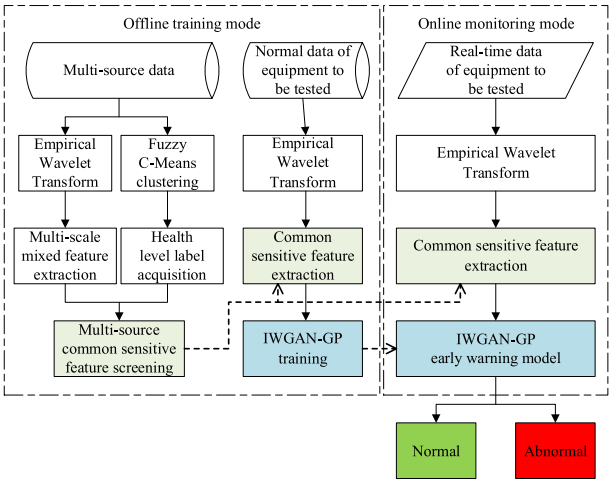

FIGURE 4. Flow chart of early fault early warning method.

Algorithm 1 Early Fault Warning Method Based on MCSF-IWGAN-GP

Offline training mode
Input: D_M, D_N
Output: $Index_{F_C}$, Model
1. $IMF_{1i}, IMF_{2i}, IMF_{3i}$= EWT (D_i), $i = 1, 2, \cdots, m$
2. F_{MSM}= FeaExt $(D_M, IMF_1, IMF_2, IMF_3)$
3. L_i = FCM (D_i), $i = 1, 2, \cdots, m$
4. $Index_{F_C}$ = MSCFS (F_{MSM}, L)
5. $IMF_{1N}, IMF_{2N}, IMF_{3N}$= EWT (D_N)
6. F_{CN} = MSCFE $\left(Index_{F_C}, D_N, IMF_{1N}, IMF_{2N}, IMF_{3N}\right)$
7. Model ← Model.fit(F_{CN})
8. return$Index_{F_C}$, Model
Online monitoring mode
Input: D_T
Output: R_{EW}
1. $IMF_{1T}, IMF_{2T}, IMF_{3T}$= EWT (D_T)
2. F_{CT} = MSCFE $\left(Index_{F_C}, D_T, IMF_{1T}, IMF_{2T}, IMF_{3T}\right)$
3. R_{EW}= Model (F_{CT})
4. returnR_{EW}

IV. EXPERIMENTAL VALIDATION

A. LABORATORY FAULT DATA VERIFICATION

1) INTRODUCTION OF BEARING LABORATORY DATASET

The XJTU-SY dataset [33] encompasses life cycle data for rolling bearings under three distinct operational conditions. The experimental setup is depicted in Fig.5. Data were sampled at a frequency of 25.6 kHz, with each sample lasting 1.28 s and sampling occurring every minute. Six datasets from three operational conditions in the XJTU-SY dataset serve as multi-source data for the screening of common sensitive features. The remaining four datasets of rolling bearing life cycle data are utilized as test data to validate the proposed method for early fault detection, as illustrated in Table 3.

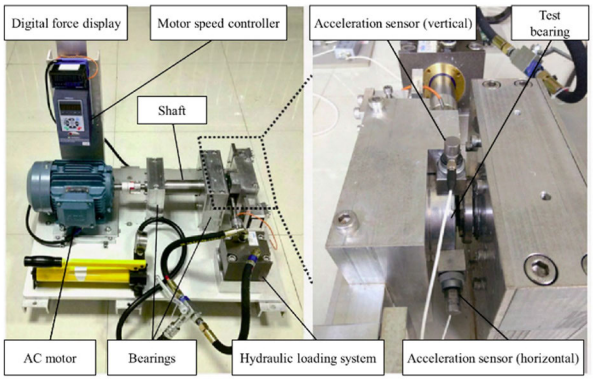

FIGURE 5. XJTU-SY test bench [33].

TABLE 3. Multi-source data and test data.

Multi-source data		Test data
Bearing 1_1	Bearing 2_2	Bearing 2_1
Bearing 1_2	Bearing 2_4	Bearing 2_3
Bearing 1_3	Bearing 3_5	Bearing 2_5
		Bearing 3_1

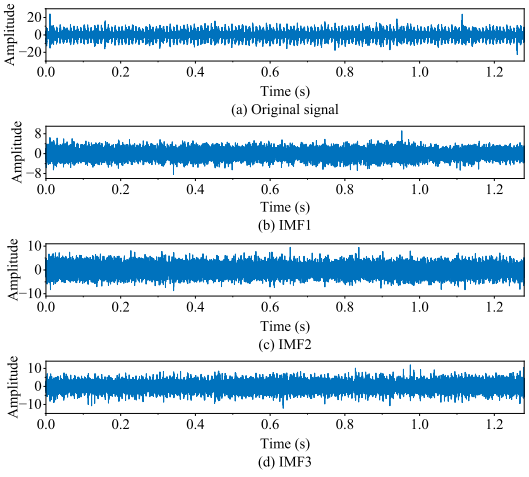

FIGURE 6. The original signal and IMF component.

2) MULTI-SCALE MIXED FEATURE EXTRACTION

The multi-source data in Table 3 are decomposed by EWT to obtain IMF1, IMF2 and IMF3.Taking Bearing 1_1 as an example, the waveform is shown in Fig.6. The

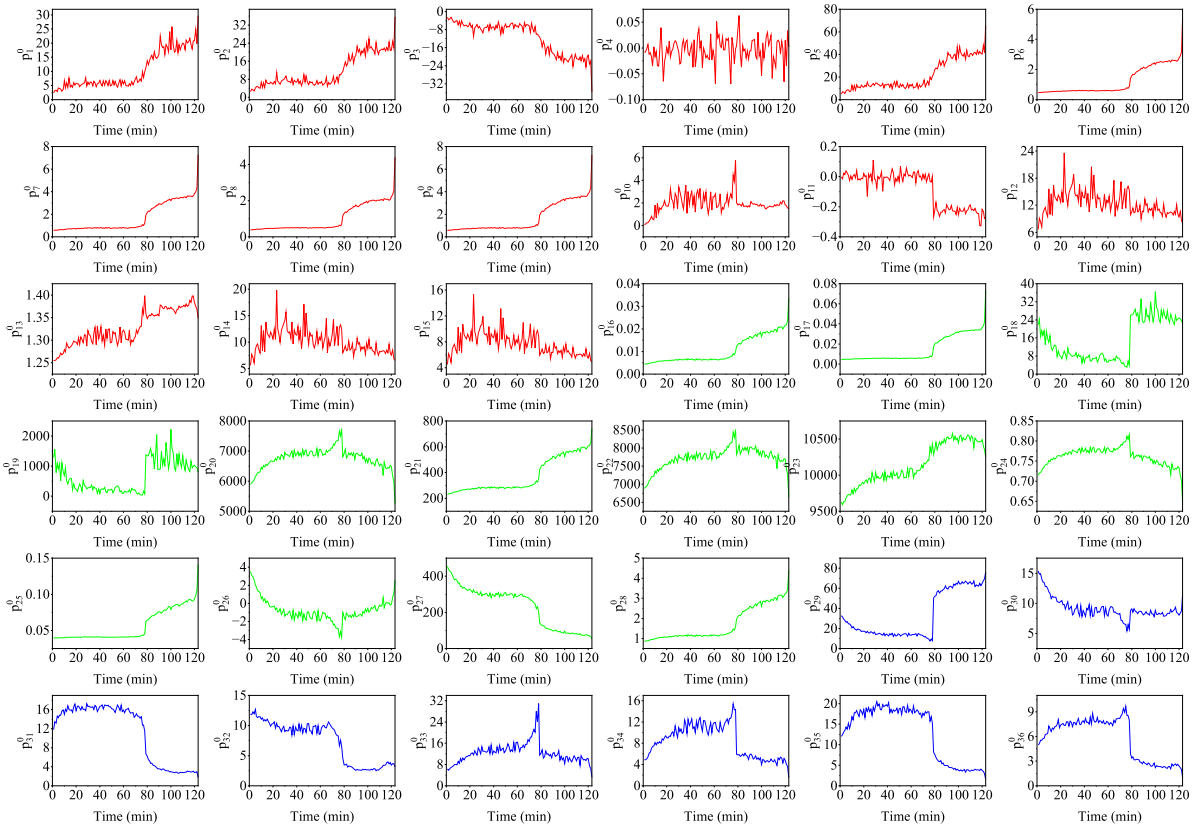

(a) Features of the original signal

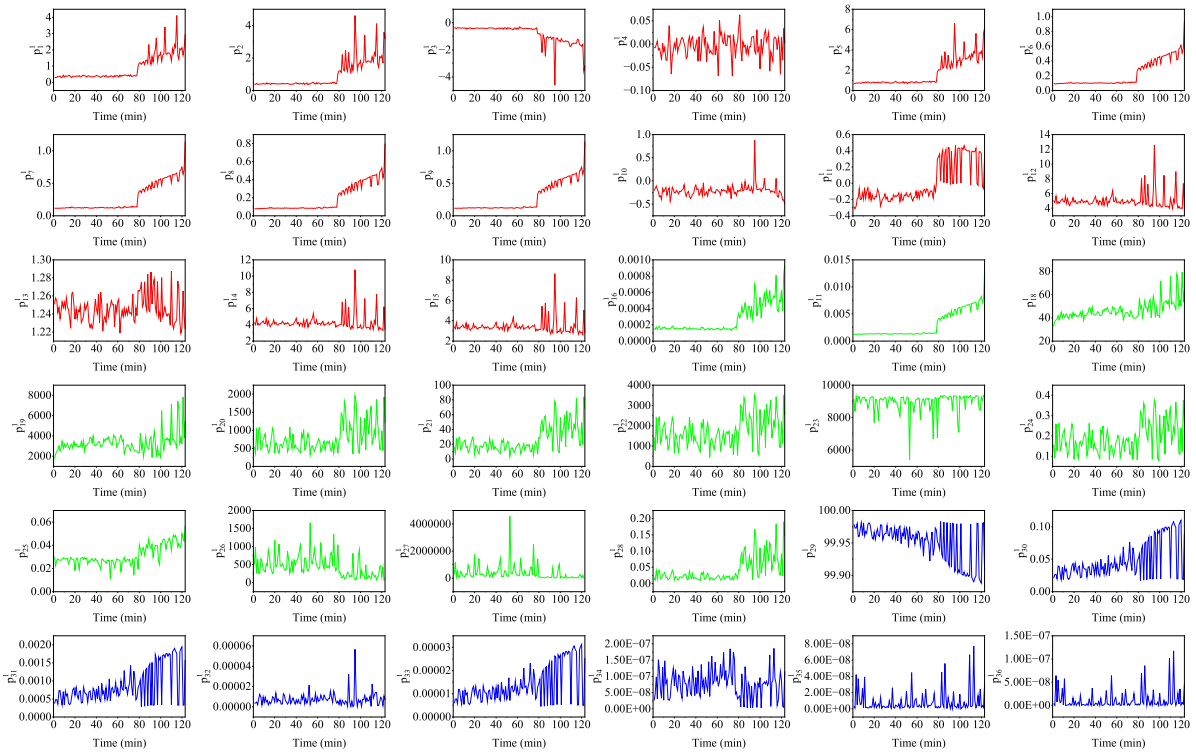

(b) Features of the IMF1

FIGURE 7. Multi-scale mixed features.

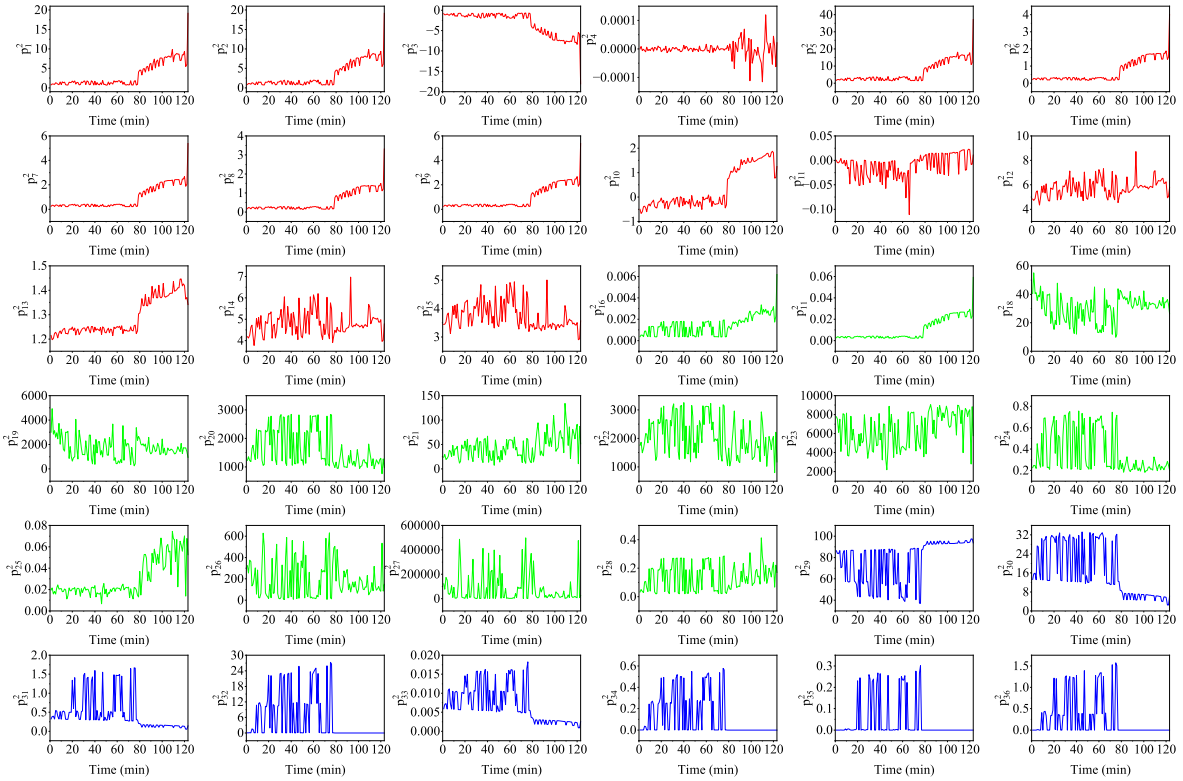

(c) Features of the IMF2

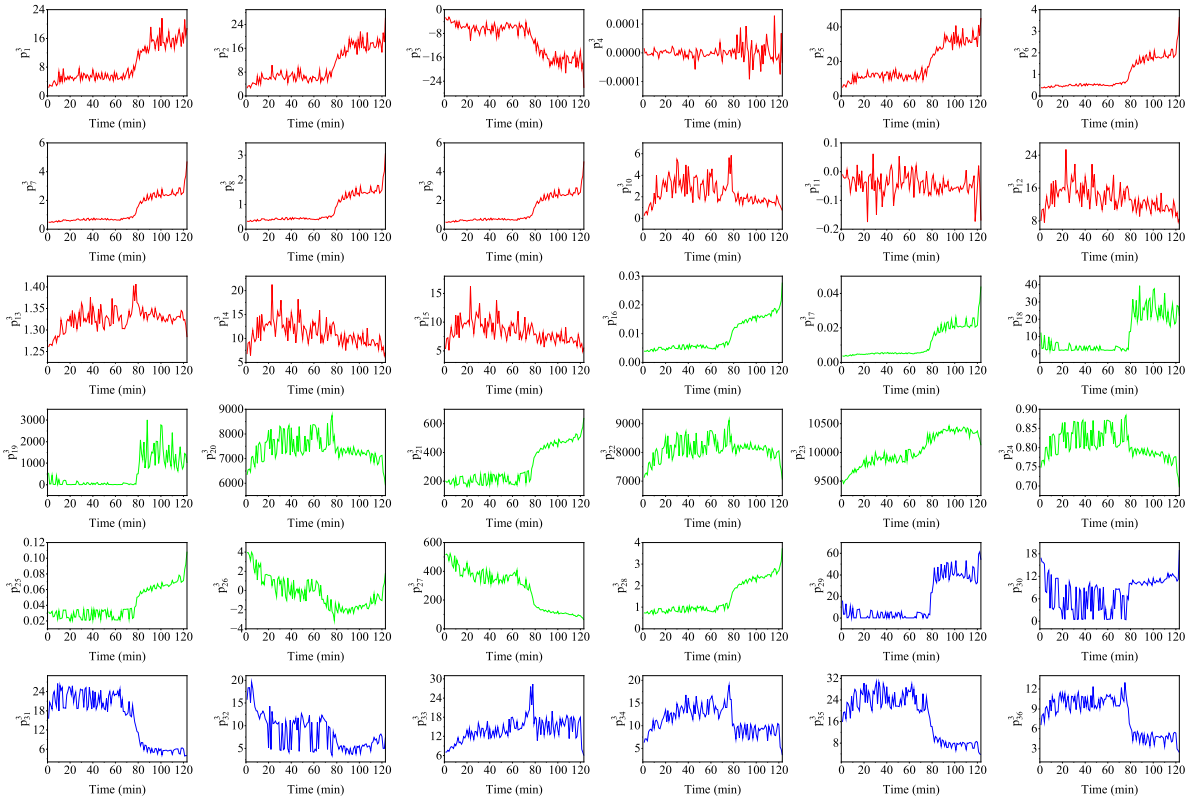

(d) Features of the IMF3

FIGURE 7. *(Continued.)* **Multi-scale mixed features.**

15 time-domain features, 13 frequency-domain features and 8 time-frequency features of the original signal and its IMF three order components are calculated respectively. The multi-scale mixed features are shown in Fig.7. The red image corresponds to 15 time-domain features, the green image corresponds to 13 frequency-domain features, and the blue image corresponds to 8 time-frequency features. Fig.7 illustrates that the time domain, frequency domain, and time-frequency domain features of the original signal, along with its IMF, prominently exhibit characteristics of early faults. However, certain features display a lack of sensitivity to these early faults. Consequently, it is imperative to identify and select those features from the multi-scale mixed features that are sensitive to early faults for effective fault diagnosis.

3) MULTI-SOURCE COMMON SENSITIVE FEATURE SCREENING

The features of early fault sensitivity should show obvious differences between normal state and abnormal state. In the multi-scale hybrid features, there are some features that have no obvious difference between normal state and abnormal state. Therefore, before using multi-scale mixed features to train the neural network, it is crucial to screen out early sensitive features, eliminate the features that have no significant difference between normal state and abnormal state, and avoid affecting the training of early fault warning model.

As shown in Fig.8, Fig.8 (a) is a feature diagram of p_1^0, Fig.8 (b) is a feature diagram of p_6^0, Fig.8 (c) is a feature diagram of p_{31}^0, and Fig.8 (d) is a feature diagram of p_{32}^0. It can be seen from the figure that although the eigenvalues are not the same, significant differences exist between the normal state and the fault state of these features. Such features are early fault sensitive features.

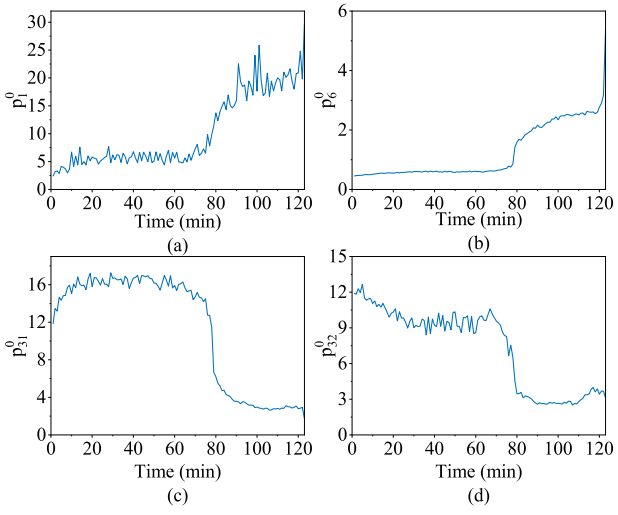

FIGURE 8. Early fault obvious features.

As shown in Fig.9, Fig.9 (a) is a feature diagram of p_4^0, Fig.9 (b) is a feature diagram of p_{10}^0, Fig.9 (c) is a feature diagram of p_{12}^0, and Fig.9 (d) is a feature diagram of p_{24}^0. The figure indicates that the features exhibit no notable distinction between the normal and fault states, characterizing them as early fault insensitive features.

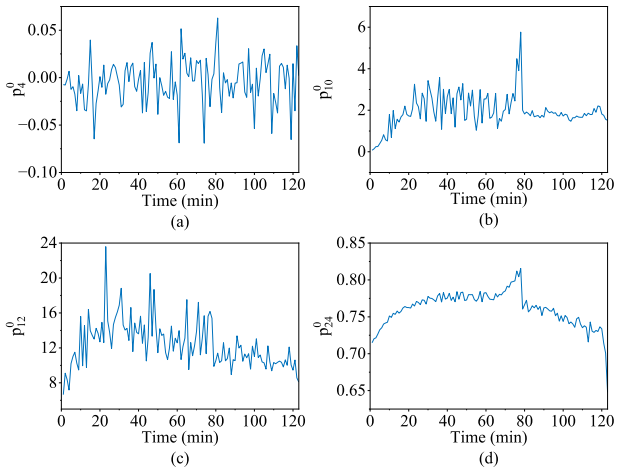

FIGURE 9. Early fault not obvious features.

The multi-source data in Table 3 is used for common sensitive feature screening. Firstly, the FCM is utilized to obtain the health level label of the multi-source data in Table 3, as shown in Fig.10. The health level label is used as the response variable of variance analysis. According to the health level label, each feature is divided into several groups, and the same health level is classified into one group.

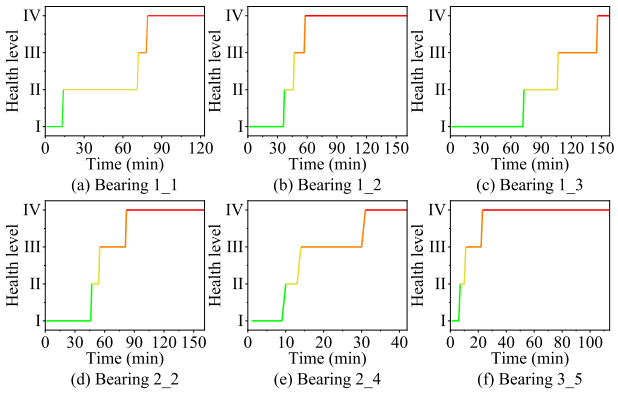

FIGURE 10. Multi-source data health level label.

According to the grouping of health levels, the F statistic is calculated by (16), and the first 36 features with the largest F statistic are taken. The results are presented in Table 4. The ranking of the selected features represents their degree of sensitivity to early faults, so the top-ranked F statistic is

given a high weight value. The value of (18) is:

$$K_{score\ i} = \begin{bmatrix} 3.6 & 3.5 & 3.4 & 3.3 & 3.2 & 3.1 \\ 3.0 & 2.9 & 2.8 & 2.7 & 2.6 & 2.5 \\ 2.4 & 2.3 & 2.2 & 2.1 & 2.0 & 1.9 \\ 1.8 & 1.7 & 1.6 & 1.5 & 1.4 & 1.3 \\ 1.2 & 1.1 & 1.0 & 0.9 & 0.8 & 0.7 \\ 0.6 & 0.5 & 0.4 & 0.3 & 0.2 & 0.1 \end{bmatrix} \tag{20}$$

TABLE 4. Multi-source data F statistics sorting.

	Multi-source data	P_{Fi}
1	Bearing 1_1	$\begin{bmatrix} p_{31}^0 & p_{29}^0 & p_{32}^0 & p_{27}^0 & p_{35}^0 & p_{36}^0 \\ p_{27}^3 & p_{21}^0 & p_{23}^0 & p_{18}^0 & p_{10}^2 & p_{11}^0 \\ p_{29}^3 & p_{23}^3 & p_{21}^3 & p_{28}^0 & p_{13}^2 & p_{28}^3 \\ p_{31}^3 & p_5^3 & p_5^0 & p_{16}^3 & p_1^0 & p_1^3 \\ p_{16}^0 & p_{34}^0 & p_2^0 & p_2^3 & p_9^3 & p_7^3 \\ p_{35}^3 & p_3^0 & p_{36}^3 & p_{25}^0 & p_{13}^0 & p_{18}^3 \end{bmatrix}$
2	Bearing 1_2	$\begin{bmatrix} p_{27}^0 & p_{27}^3 & p_{32}^0 & p_{30}^0 & p_{30}^3 & p_{32}^3 \\ p_{31}^0 & p_{23}^3 & p_{25}^0 & p_{23}^0 & p_{21}^0 & p_{21}^3 \\ p_{25}^3 & p_{28}^0 & p_9^0 & p_7^0 & p_6^0 & p_8^0 \\ p_{17}^0 & p_{31}^3 & p_{28}^3 & p_2^0 & p_5^0 & p_{26}^3 \\ p_3^0 & p_7^3 & p_9^3 & p_6^3 & p_5^3 & p_8^3 \\ p_{17}^3 & p_2^3 & p_1^0 & p_{16}^0 & p_3^3 & p_1^3 \end{bmatrix}$
3	Bearing 1_3	$\begin{bmatrix} p_{31}^0 & p_{29}^0 & p_{32}^0 & p_{27}^0 & p_{35}^0 & p_{36}^0 \\ p_{27}^3 & p_{21}^0 & p_{23}^0 & p_{18}^0 & p_{10}^2 & p_{11}^0 \\ p_{29}^3 & p_{23}^3 & p_{21}^3 & p_{28}^0 & p_{13}^2 & p_{28}^3 \\ p_{31}^3 & p_5^3 & p_5^0 & p_{16}^3 & p_1^0 & p_1^3 \\ p_{16}^0 & p_{34}^0 & p_2^0 & p_2^3 & p_9^3 & p_7^3 \\ p_{35}^3 & p_3^0 & p_{36}^3 & p_{25}^0 & p_{13}^0 & p_{18}^3 \end{bmatrix}$
4	Bearing 2_2	$\begin{bmatrix} p_{27}^0 & p_{35}^0 & p_{31}^0 & p_{21}^0 & p_3^0 & p_5^0 \\ p_{36}^0 & p_5^3 & p_3^3 & p_2^0 & p_{25}^0 & p_2^3 \\ p_{29}^0 & p_{28}^0 & p_9^0 & p_7^0 & p_{17}^0 & p_6^0 \\ p_8^0 & p_7^3 & p_9^3 & p_{16}^3 & p_{17}^3 & p_1^3 \\ p_6^3 & p_{28}^3 & p_1^0 & p_8^3 & p_{16}^3 & p_{17}^2 \\ p_7^2 & p_9^2 & p_6^2 & p_8^2 & p_{32}^0 & p_{21}^3 \end{bmatrix}$
5	Bearing 2_4	$\begin{bmatrix} p_{27}^0 & p_{27}^3 & p_{31}^0 & p_{35}^0 & p_{36}^0 & p_{21}^0 \\ p_{25}^0 & p_{29}^0 & p_{21}^3 & p_{34}^0 & p_{28}^0 & p_{23}^3 \\ p_{28}^3 & p_{25}^3 & p_8^2 & p_{32}^0 & p_6^2 & p_{31}^3 \\ p_{35}^3 & p_8^0 & p_{33}^0 & p_{23}^0 & p_{16}^2 & p_7^2 \\ p_9^2 & p_{17}^2 & p_6^0 & p_{16}^0 & p_5^3 & p_{16}^3 \\ p_9^0 & p_7^0 & p_3^3 & p_{17}^0 & p_{36}^3 & p_5^0 \end{bmatrix}$
6	Bearing 3_5	$\begin{bmatrix} p_{27}^3 & p_{27}^0 & p_{26}^3 & p_{33}^0 & p_{33}^3 & p_{25}^3 \\ p_{25}^0 & p_{17}^3 & p_7^3 & p_9^3 & p_{22}^3 & p_6^3 \\ p_8^3 & p_{21}^3 & p_{21}^0 & p_{36}^0 & p_{17}^0 & p_8^0 \\ p_6^0 & p_7^0 & p_9^0 & p_{20}^3 & p_5^3 & p_3^3 \\ p_{13}^3 & p_2^3 & p_{24}^3 & p_{28}^3 & p_1^3 & p_{28}^0 \\ p_{29}^0 & p_{30}^0 & p_{35}^0 & p_{24}^2 & p_{16}^0 & p_{16}^3 \end{bmatrix}$

The weight values of (20) are sorted according to the F statistic of multi-source data in Table 4, and the weight values are given respectively. For example, the F statistic calculated by the Bearing 1_1 data ranks the first as p_{31}^0 feature and the 36th as p_{18}^3, then the weight value of p_{31}^0 is given to be 3.6, and the weight value of p_{18}^3 is given to be 0.1. The sensitive feature weight values of multi-source data are superimposed to calculate the sensitive score matrix. Fig.11 displays the sensitivity scores for 144 multi-scale mixed features. The top 16 features with the highest sensitivity scores are identified as multi-source common sensitive features. The multi-source common sensitive features are extracted from the test data in Table 3. Taking the Bearing 2_1 data as an example, the multi-source common sensitive features are shown in Fig.12.

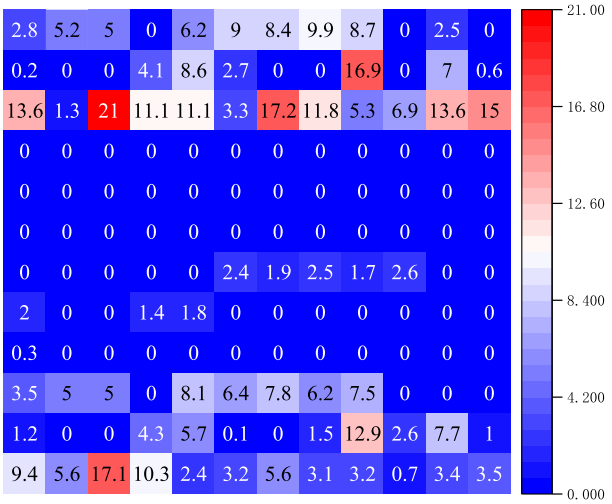

FIGURE 11. Sensitive score matrix.

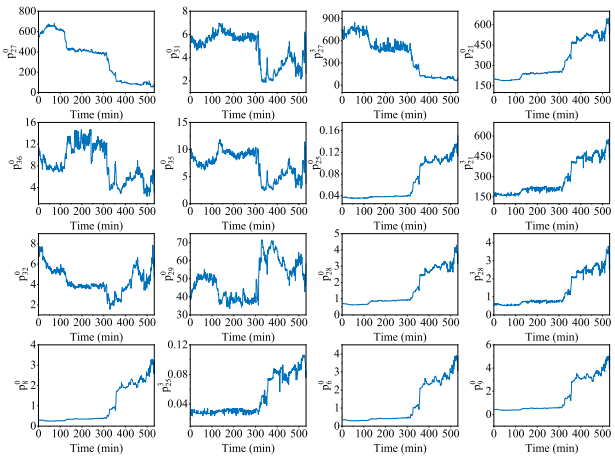

FIGURE 12. Bearing 2_1 early fault sensitive features.

4) IWGAN-GP TRAINING AND TESTING

The IWGAN-GP model utilizes solely the normal data from the equipment under test for its training samples. The first 100 sets of data in Table 3 are taken as the normal data, and the multi-source common sensitive features are extracted as the training samples of IWGAN-GP. As shown in Table 5, the IWGAN-GP generator constructed in this paper uses three two-dimensional deconvolution layers. The filters are set to 32, 16, and 1, the convolution kernel size is (3, 3), (4, 4), and (4, 4), and the strides is 1, 2, and 2, respectively. Following three deconvolution layers, a Flatten operation is applied,

after which the output of the fully connected layer is utilized with 16 neurons. All generator's layers use the ReLU activation function. The discriminator uses three two-dimensional convolution layers. The filters are set to 16, 32, and 64, the convolution kernel size is (3, 3), (3, 3), and (3, 3), and the strides is 1, 2, and 2, respectively. The Dropout layer is used after each convolutional layer, and the forgetting rate is set to 0.5. Before the first convolution layer, the input adaptive layer is used to convert the training samples from (100, 16) to (100, 28, 28). After the last convolution layer, Flatten is performed, and then the fully connected layer output is used, and the neuron is 1. In addition to the full connection layer using the Sigmoid activation function, the rest all use the LeakyReLU activation function. Both the generator and discriminator employ the Adam optimizer, with learning rates of 10^{-4} and 2×10^{-4}, respectively. The batch size is established at 16. The incorporation of the Wasserstein distance and gradient penalty into the model ensures that the generator's gradient remains stable, even when the discriminator achieves high accuracy. Therefore, the generator is optimized once for every 5 discriminators.

TABLE 5. Parameters of IWGAN-GP.

Model	Structure	Parameters		
		filter	kernel size	strides
Generator	Input		16	
	Dense		3136	
	Reshape		(7, 7, 64)	
	Conv2DTranspose	32	(3, 3)	1
	ReLU			
	Conv2DTranspose	16	(4, 4)	2
	ReLU			
	Conv2DTranspose	1	(4, 4)	2
Discriminator	Flatten			
	Dense		16	
	ReLU			
	Input		16	
	Input Adaptive Layer		(28, 28, 1)	
	LeakyReLU			
	Conv2D	16	(3, 3)	1
	LeakyReLU			
	Dropout		0.5	
	Conv2D	32	(3, 3)	2
	LeakyReLU			
	Dropout		0.5	
	Conv2D	64	(3, 3)	2
	LeakyReLU			
	Dropout		0.5	
	Flatten			
	Dense		1	
	Sigmoid			

The early fault warning test results of the test data in Table 3 are depicted in Fig.13. Fig.13 (a) is the early fault warning result of Bearing 2_1, with a total of 491 sets of data files. The proposed method realizes early warning at the 453rd set of data files. Fig.13 (b) is the early fault warning result of Bearing 2_3, with a total of 533 sets of data files. The proposed method realizes early warning at the 128th set of data files. Fig.13 (c) is the early fault warning result of Bearing 2_5, with a total of 339 sets of data files. The proposed method realizes early warning at the 123rd set of data files. Fig.13 (d) is the early fault warning result of Bearing 3_1, with a total of 2538 sets of data files. The proposed method realizes early warning at the 2387th set of data files. The acceleration RMS curve depicted in the diagram intuitively displays the bearing's performance degradation trend. The proposed method realizes the alarm before the serious deterioration of the fault.

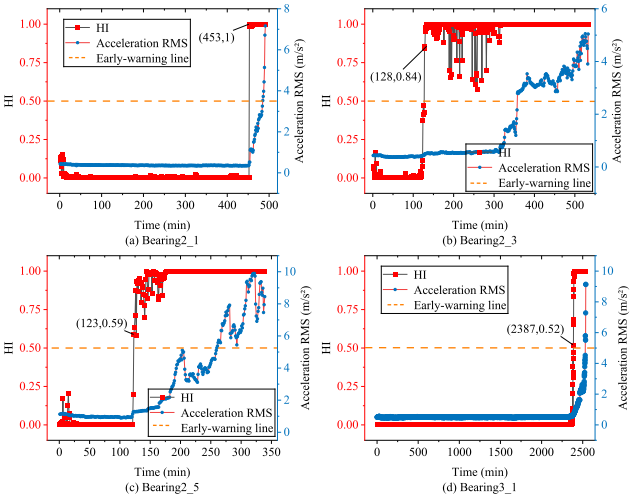

FIGURE 13. Early fault warning test results.

B. ENGINEERING CASE DATA VERIFICATION

1) CENTRIFUGAL PUMP BEARING ENGINEERING CASE DATA VERIFICATION

The methodology presented in this study has been validated using the engineering case data from a P3409A centrifugal pump bearing failure at a petrochemical plant. The location of the vibration sensor on the centrifugal pump bearing is depicted in Fig.14. The pump operates at a rotational speed of 2980 r/min, with a sampling frequency set at 25.6 kHz. Sampling was performed once every 2 hours, and the data length was 16384.

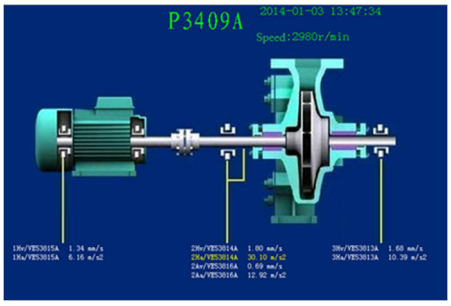

FIGURE 14. P3409A pump measuring point diagram.

There are 332 sets of data files in this project case. The previous 100 sets of data files are used as normal data. The multi-source common sensitive features are extracted to train

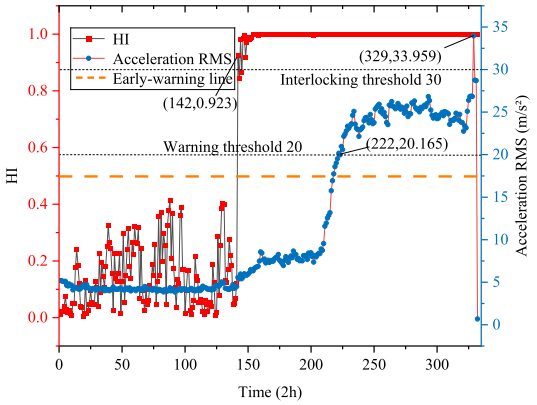

FIGURE 15. Centrifugal pump bearing engineering case data early fault early warning results.

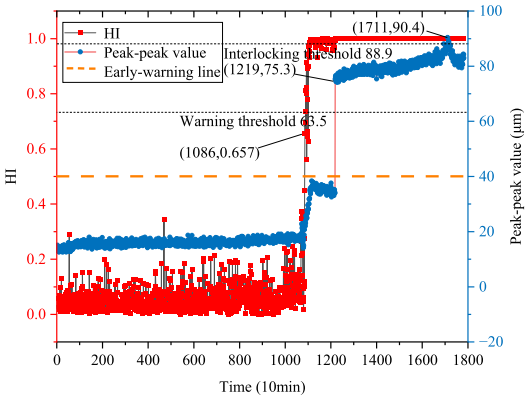

FIGURE 17. Centrifugal compressor rotor imbalance fault case.

IWGAN-GP, and the discriminator is used as an early warning model to test 332 sets of life-cycle data. The results are shown in Fig.15. The proposed method realizes early warning at 142 sets of data files, which is $(222-142)\times 2=160h$ earlier than the fixed threshold line alarm method widely used in industry.

2) CENTRIFUGAL COMPRESSOR ROTOR SYSTEM ENGINEERING CASE DATA VALIDATION

Fig.16 is a project case of a circulating hydrogen centrifugal compressor rotor system in a petrochemical company. The rotor fouling causes the rotor to be unbalanced. The speed is 12100 r/min, and the data are collected every 10 min.

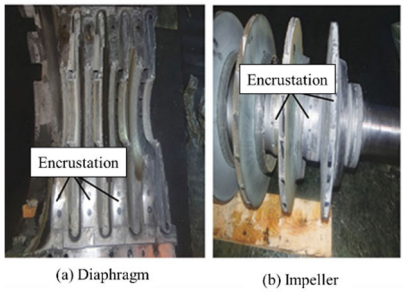

FIGURE 16. Centrifugal compressor rotor imbalance fault case.

There are 1782 sets of data files in this project case. The previous 200 sets of data are normal data. The multi-source common sensitive features are extracted to train IWGAN-GP, and the discriminator is used as an early warning model to test 1782 sets of life-cycle data. The results are shown in Fig.17. The proposed method realizes early warning at 1086 sets of data files, which is $(1219-1068)\times 10=1330min$ ahead of the fixed threshold line alarm method.

V. METHODS COMPARISON

The proposed method is compared with the published early fault warning methods L1TF-SVDD [14] and AE-GAN [19]. L1TF-SVDD extracts the spectral distance index and multi-scale dispersion entropy of normal data, and uses the improved L1 trend filtering method to obtain the trend factor with less fluctuation. According to the characteristics of training data, the kernel function bandwidth of SVDD is determined and the SVDD model is trained. In the SVDD model, the distance from the real-time data trend factor to the hypersphere's center serves as a health indicator for early fault warning. The L1TF-SVDD model structure is shown in Fig.18. AE-GAN integrates an autoencoder with a generative adversarial network, utilizing normal data training to refine the adversarial network. This enables the generator to accurately reconstruct the normal data distribution. Subsequently, the trained generator functions as a decoder, coupled with an auxiliary encoder, to establish an autoencoder module. The reconstruction error produced by this autoencoder serves as a health indicator for early fault warning. The AE-GAN model structure is shown in Fig.19.

The open bearing life data set XJTU-SY dataset [33] is used as the test and verification data of the three comparison methods. The Bearing 2_1, Bearing 2_3, Bearing 2_5 and Bearing 3_1 in the XJTU-SY dataset, and the previous 100 sets of normal data are used as the training data of the model. The L1TF-SVDD, AE-GAN and the proposed method MCSF-IWGAN-GP are used for model verification.

Bearing 2_1 has a total of 491 sets of data, and the model verification results are shown in Fig.20. Fig.20 (a) shows the verification results of L1TF-SVDD. The warning line is HI=0.267, and the model alarms at the 456th group of data. Fig.20 (b) is the verification result of AE-GAN, the warning line is HI=0.182, and the model alarms at the 453rd set of data. Fig.20 (c) shows the verification results of the proposed method MCSF-IWGAN-GP. The warning line is HI=0.5, and the model alarms at the 453rd group of data.

Bearing 2_3 has a total of 533 sets of data, and the model verification results are shown in Fig.21. Fig.21 (a) shows the verification results of L1TF-SVDD. The warning line is HI=0.102, and the model alarms at the 324th set of data. Fig.21 (b) is the verification result of AE-GAN, the warning line is HI=0.198, and the model alarms at the 128th set of data. Fig.21 (c) is the verification result of the proposed

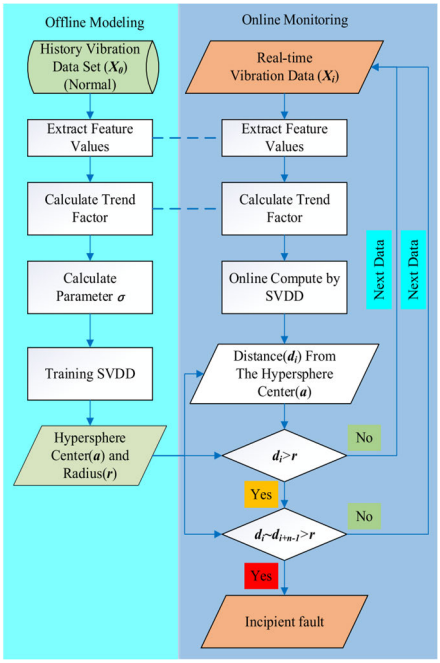

FIGURE 18. L1TF-SVDD structure diagram [14].

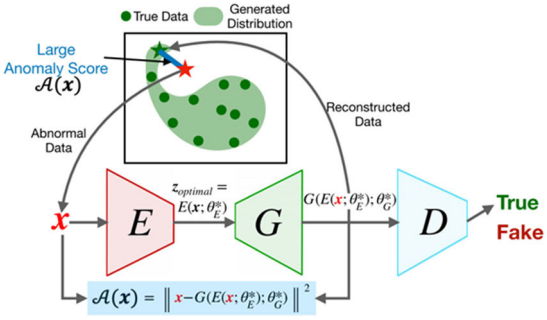

FIGURE 19. AE-GAN structure diagram [19].

method MCSF-IWGAN-GP. The warning line is HI=0.5, and the model alarms at the 128th set of data.

There are 339 sets of data in Bearing 2_5, and the model verification results are shown in Fig.22. Fig.22 (a) is the verification result of L1TF-SVDD, the warning line is HI=0.146, and the model alarms at the 184th set of data. Fig.22 (b) is the verification result of AE-GAN, the warning line is HI=1.290, and the model alarms at the 122nd set of data. Fig.22 (c) is the verification result of the proposed method MCSF-IWGAN-GP. The warning line is HI=0.5, and the model alarms at the 123rd set of data.

There are 2538 sets of data in Bearing 3_1, and the model verification results are shown in Fig.23. Fig.23 (a) shows the verification results of L1TF-SVDD. The warning line is HI=0.230, and the model alarms at the 2396th group of data. Fig.23 (b) is the verification result of AE-GAN, the warning line is HI=0.295, and the model alarms at the 2344th set of data. Fig.23 (c) is the verification result of the proposed method MCSF-IWGAN-GP. The warning line is HI=0.5, and the model alarms at the 2387th set of data.

In order to verify that the early fault warning results are credible, the envelope spectrum analysis is performed on the data before and after the early fault warning point to find the first early fault point with fault characteristic frequency. Bearing 2_1 presents fault data for the inner ring, with a theoretical fault characteristic frequency of 184.4 Hz. The envelope spectrum of the 453rd data set, as depicted in Fig.24, exhibits frequency components at 179.7 Hz and its harmonic, closely aligning with the theoretical fault frequency. Bearing 2_3, representing cage fault data, has a theoretical fault characteristic frequency of 14.5 Hz. Fig.25 displays the envelope spectrum for the 130th data set, featuring frequency components at 13.3 Hz and its harmonic, aligning closely with the theoretical fault characteristic frequency. Moreover, these frequency components were also present in the 128th data set's envelope spectrum. Bearing 2_5, representing outer ring fault data, has a theoretical fault characteristic frequency of 115.6 Hz. Correspondingly, Fig.26 illustrates that the 121st data set's envelope spectrum contains frequency components at 118 Hz and its harmonic, which approximate the theoretical fault characteristic frequency. Similarly, Bearing 3_1, another outer ring fault data set, has a theoretical fault characteristic frequency of 123.3 Hz. This is corroborated by Fig.27, where the envelope spectrum of the 2376th data set includes frequency components at 124.2 Hz and its harmonic, nearing the theoretical fault characteristic frequency.

Through the above comparative test, the following conclusions can be drawn:

(1) The early fault warning effect of MCSF-IWGAN-GP and AE-GAN is better than that of L1TF-SVDD. In the model verification tests of Bearing 2_1, Bearing 2_3, Bearing 2_5 and Bearing 3_1, the early fault warning results of the proposed methods MCSF-IWGAN-GP and AE-GAN are earlier than those of L1TF-SVDD, as shown in Table 6. The trend of performance degradation in bearings can be clearly observed through the acceleration RMS curve. Both the proposed methods MCSF-IWGAN-GP and AE-GAN achieve alarm before the fault deteriorates seriously.

(2) The proposed method MCSF-IWGAN-GP is superior to AE-GAN and L1TF-SVDD in distinguishing normal and abnormal health indicators. As shown in Table 7, calculate the average value of health indicators HI of normal data before the warning point, and the ratio of the average value of health indicators of normal data to the health indicators of the warning point $\bar{HI}$ /HI%, the greater the ratio, the smaller the discrimination between normal and abnormal health indicators. The health indicators of AE-GAN and L1TF-SVDD normal data are less different from those of early faults. The health indicators gradually increase with the severity of faults, while the health indicators of the normal data of the proposed method are different from those of early faults.

(3) The false alarm rate for MCSF-IWGAN-GP is lower compared to AE-GAN and L1TF-SVDD. Referring to Table 8, the ratio of the average health indicator values for

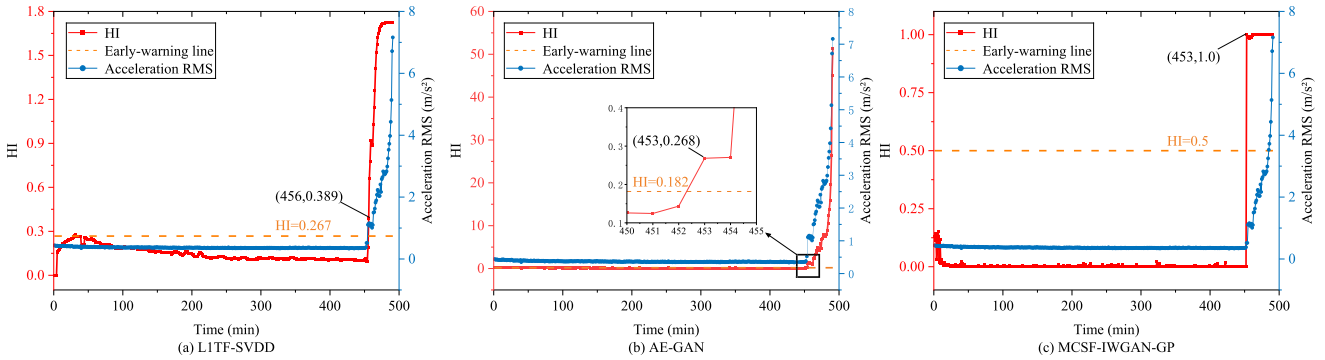

FIGURE 20. Model verification results of Bearing 2_1.

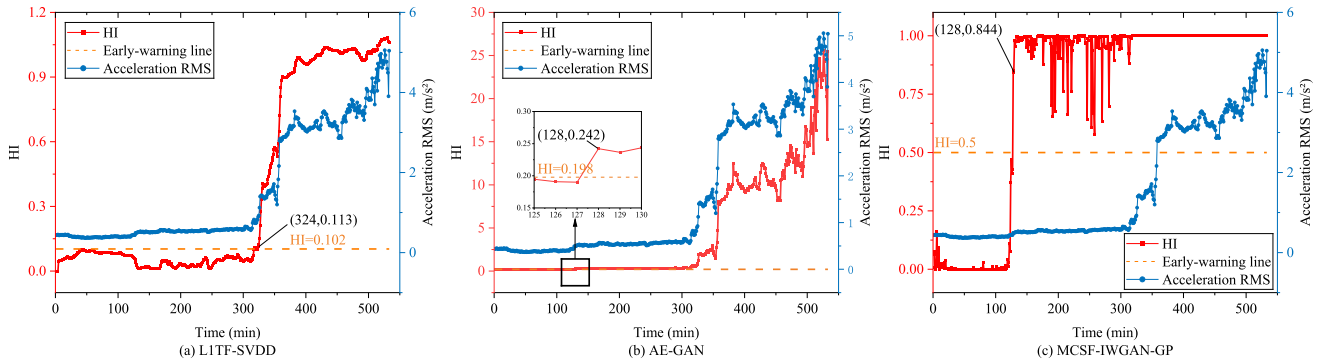

FIGURE 21. Model verification results of Bearing 2_3.

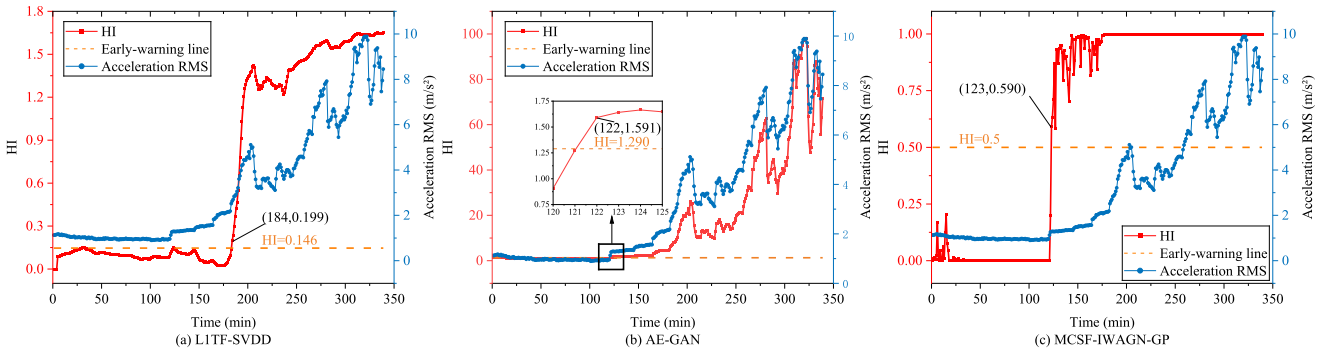

FIGURE 22. Model verification results of Bearing 2_5.

TABLE 6. Multi-source data F statistics sorting.

Test data	Early fault point	Early fault warning point		
		L1TF-SVDD	AE-GAN	Proposed method
Bearing 2_1	453	456	453	453
Bearing 2_3	130	324	128	128
Bearing 2_5	121	184	122	123
Bearing 3_1	2376	2396	2344	2387

normal data to the health indicators at the early warning threshold is represented as $\overline{HI}/\mathrm{HI}\%$. The greater the ratio, the closer the early warning line is to the health indicators of the normal data. It can be seen from Fig.20 to Fig.23 that the early warning lines of AE-GAN and L1TF-SVDD are very close to the health index HI of normal data. When the

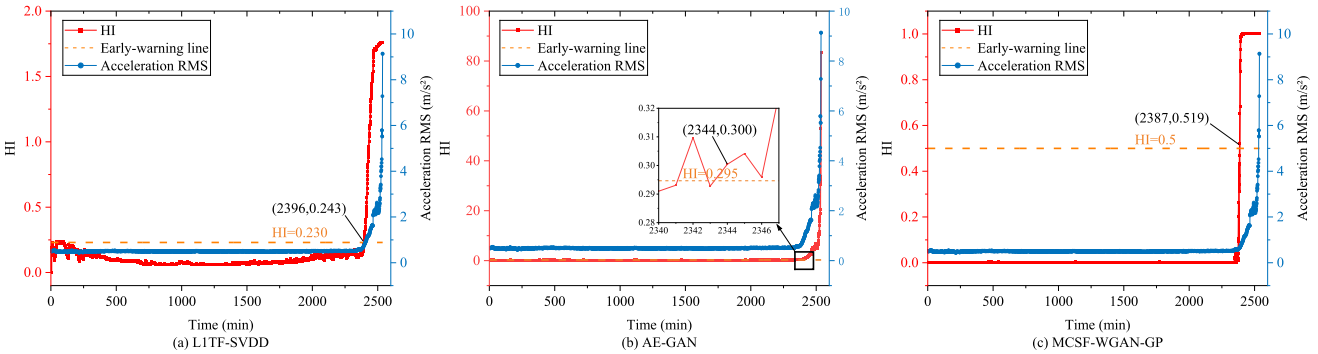

FIGURE 23. Model verification results of Bearing 3_1.

TABLE 7. Discrimination between normal and abnormal health indicators.

Test data	L1TF-SVDD			AE-GAN			Proposed method		
	Normal data $\overline{HI}$	Warning point HI	$\overline{HI}$/HI %	Normal data $\overline{HI}$	Warning point HI	$\overline{HI}$/HI %	Normal data $\overline{HI}$	Warning point HI	$\overline{HI}$/HI %
Bearing 2_1	0.149	0.389	38.3	0.135	0.268	50.4	0.004	1.0	0.4
Bearing 2_3	0.054	0.113	47.8	0.160	0.242	66.1	0.022	0.844	2.6
Bearing 2_5	0.094	0.199	47.2	0.983	1.591	61.8	0.009	0.590	1.5
Bearing 3_1	0.100	0.243	41.2	0.236	0.300	82.0	0.002	0.519	0.3

TABLE 8. The ratio of normal data $\overline{HI}$ to early warning line HI.

Test data	L1TF-SVDD			AE-GAN			Proposed method		
	Normal data $\overline{HI}$	Early-warning line HI	$\overline{HI}$/HI %	Normal data $\overline{HI}$	Early-warning line HI	$\overline{HI}$/HI %	Normal data $\overline{HI}$	Early-warning line HI	$\overline{HI}$/HI %
Bearing 2_1	0.149	0.267	55.8	0.135	0.182	74.2	0.004	0.5	0.8
Bearing 2_3	0.054	0.102	52.9	0.160	0.198	80.8	0.022	0.5	4.4
Bearing 2_5	0.094	0.146	64.4	0.983	1.290	76.2	0.009	0.5	1.8
Bearing 3_1	0.100	0.230	43.5	0.236	0.295	80.0	0.002	0.5	0.4

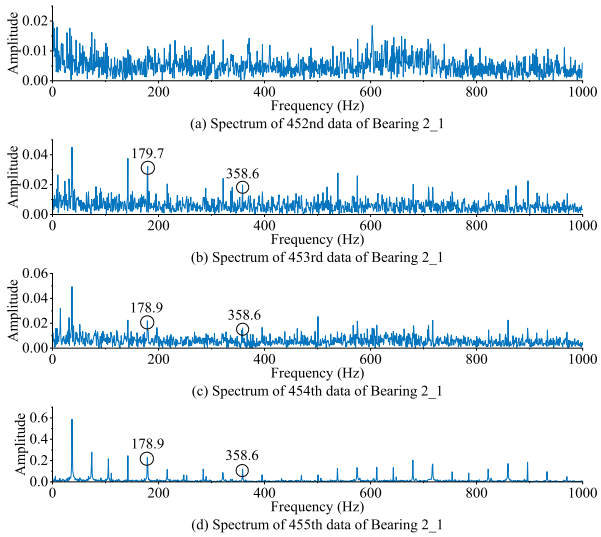

FIGURE 24. Envelope analysis of Bearing 2_1.

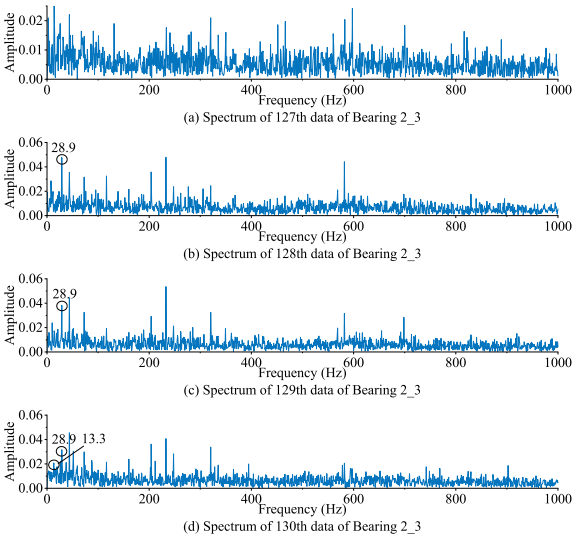

FIGURE 25. Envelope analysis of Bearing 2_3.

operating conditions fluctuate, the health index is easy to exceed the early warning line and false alarm occurs. However, the warning line of the proposed method is greatly different from the health index of normal data, and there

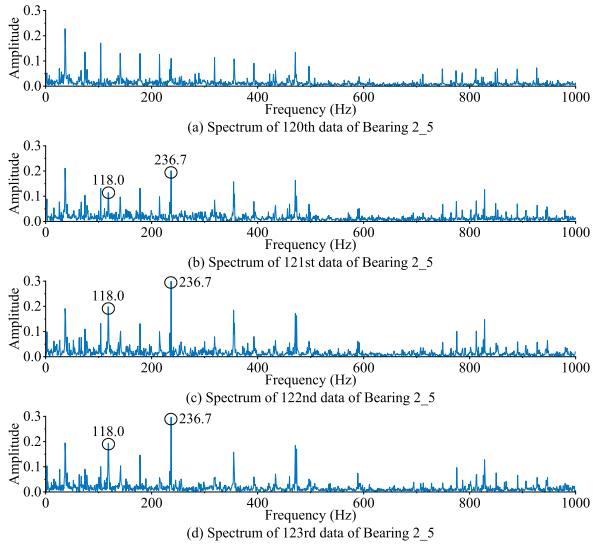

FIGURE 26. Envelope analysis of Bearing 2_5.

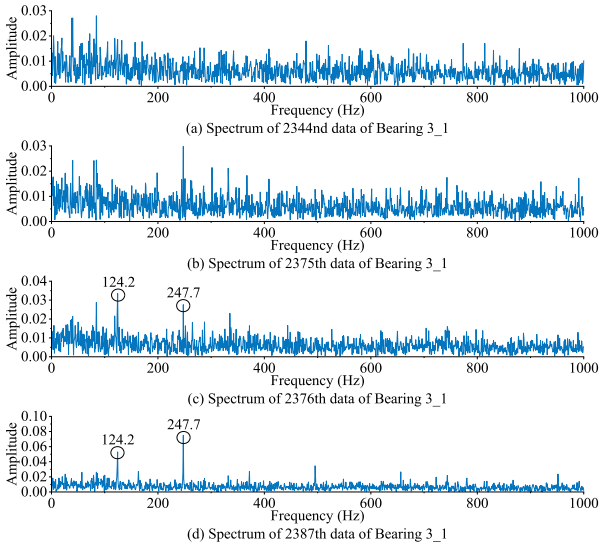

FIGURE 27. Envelope analysis of Bearing 3_1.

are few false alarms due to the fluctuation of operating conditions.

VI. CONCLUSION

Aiming at the problems that it is difficult to screen multi-source common sensitive features, difficult training of neural network with small number of sensitive features, and WGAN-GP is difficult to be directly used for early fault warning, an early fault warning method for rotating machinery based on MCSF-IWGAN-GP is proposed. The proposed method is verified by XJTU-SY bearing laboratory data, centrifugal pump bearing fault engineering case data and centrifugal compressor rotor system engineering case. The conclusions are as follows:

(1) Using XJTU-SY bearing laboratory data Bearing 1_1, Bearing 1_2, Bearing 1_3, Bearing 2_2, Bearing 2_4, Bearing 3_5 multi-source data, the multi-source common sensitive features with generalization can be screened out by the feature screening method based on variance analysis F test proposed in this paper.

(2) The IWGAN-GP model is constructed, which can complete the discrimination of normal and abnormal with a small number of sensitive features, and realize early fault warning. The discriminator structure is improved. The input adaptive layer added to the network structure can map a small number of sensitive features to high-dimensional features to complete the learning of the neural network. The training function of WGAN-GP is improved, and the original discrimination of true or false samples of the discriminator is improved to the discrimination of normal or abnormal samples, which is successfully applied to the early fault warning of rotating machinery. The equipment under test can complete the training of the model only by providing historical normal data.

(3) The proposed method has realized the alarm on the XJTU-SY bearing laboratory data Bearing 2_1, Bearing 2_3, Bearing 2_5 and Bearing 3_1 before the serious deterioration of the fault. The proposed method is applied to the fault engineering case data of P3409A centrifugal pump bearing in a petrochemical company, and the alarm is 160 h earlier than the fixed threshold line alarm method widely used in industry. On the case data of SC petrochemical company 's circulating hydrogen centrifugal compressor rotor system engineering, the proposed method alarms 1330 min earlier than the fixed threshold line alarm method.

(4) Compared with the two published methods L1TF-SVDD and AE-GAN, the proposed method has better early fault warning effect, better normal and abnormal health index discrimination and less false alarm by comparing tests on XJTU-SY bearing laboratory data Bearing 2_1, Bearing 2_3, Bearing 2_5, and Bearing 3_1.

In future studies, we will use more engineering case data to verify the proposed method.

REFERENCES

[1] J. Yang, Y. Yang, and G. Xie, "Diagnosis of incipient fault based on sliding-scale resampling strategy and improved deep autoencoder," *IEEE Sensors J.*, vol. 20, no. 15, pp. 8336–8348, Aug. 2020.

[2] J. Tian, X. Gao, R. Chen, F. Zhang, and Z. Wang, "Rolling bearing fault early warning method based on beta distribution and filtering noise reduction algorithm," *Chin. J. Sci. Instrum.*, vol. 44, no. 12, pp. 44–54, 2023.

[3] J. Guo, Z. Si, and J. Xiang, "Cycle kurtosis entropy guided symplectic geometry mode decomposition for detecting faults in rotating machinery," *ISA Trans.*, vol. 138, pp. 546–561, Jul. 2023.

[4] T. Wang, C. Chen, Y. Luo, S. Zhao, and S. Huang, "Initial fault diagnosis of bearing based on AVMD-SE and multiscale enhanced morphological top-hat filter," *J. Mech. Sci. Technol.*, vol. 36, no. 12, pp. 6289–6305, Dec. 2022.

[5] B. Xu and H. Li, "A novel empirical variational mode decomposition for early fault feature extraction," *IEEE Access*, vol. 10, pp. 134826–134847, 2022.

[6] X. Sun, H. Liu, X. Zhao, and B. Zhou, "Singular point recognition and feature extraction of early fault of rolling bearing based on instantaneous envelope scale spectrum entropy," *Chin. J. Mech. Eng.*, vol. 53, no. 3, pp. 73–80, 2017.

[7] R. Yang, H. Li, C. He, and F. Wang, "Early fault feature extraction of rolling bearing based on optimal wavelet scale cyclic spectrum," *Chin. J. Mech. Eng.*, vol. 54, no. 17, pp. 208–217, 2018.

[8] R. Liu, B. Yang, X. Zhang, S. Wang, and X. Chen, "Time-frequency atoms-driven support vector machine method for bearings incipient fault diagnosis," *Mech. Syst. Signal Process.*, vol. 75, pp. 345–370, Jun. 2016.

[9] J. Cheng, Y. Yang, X. Li, H. Pan, and J. Cheng, "An early fault diagnosis method of gear based on improved symplectic geometry mode decomposition," *Measurement*, vol. 151, Feb. 2020, Art. no. 107140.

[10] Y. Shi, Y. Liu, and X. Gao, "Study of wind turbine fault diagnosis and early warning based on SCADA data," *IEEE Access*, vol. 9, pp. 124600–124615, 2021.

[11] Y. Xiao, Q. Wang, Z. Yang, W. Xu, Y. Shu, and W. Chen, "Research on early warning and diagnosis method of sudden unbalance fault of rotating machinery," *Chin. J. Mech. Eng.*, vol. 59, no. 11, pp. 308–318, 2023.

[12] Q. Wang, B. Wei, J. Liu, W. Ma, and S. Xu, "Research on the construction and application of a data-driven early fault detection model for rotating machinery," *Chin. J. Mech. Eng.*, vol. 56, no. 16, pp. 22–32, 2020.

[13] Y. Kang, G. Chen, H. Wang, W. Pan, and X. Wei, "Early fault warning of rolling bearing based on self-supervised deep one-class classification," to be published.

[14] Q. Wang, X. Liu, B. Wei, and W. Chen, "Online incipient fault detection method based on improved l1 trend filtering and support vector data description," *IEEE Access*, vol. 9, pp. 30043–30059, 2021.

[15] G. Liu, H. Gu, X. Shen, and D. You, "Bayesian long short-term memory model for fault early warning of nuclear power turbine," *IEEE Access*, vol. 8, pp. 50801–50813, 2020.

[16] Z. Gao, Y. Liu, Q. Wang, J. Wang, and Y. Luo, "Ensemble empirical mode decomposition energy moment entropy and enhanced long short-term memory for early fault prediction of bearing," *Measurement*, vol. 188, Jan. 2022, Art. no. 110417.

[17] X. Peng, T. Peng, C. Yang, C. Ye, Z. Chen, and C. Yang, "Adversarial domain adaptation network with MixMatch for incipient fault diagnosis of PMSM under multiple working conditions," *Knowl.-Based Syst.*, vol. 284, Jan.25, 2024, Art. no. 111331.

[18] Y. Ding, J. Zhuang, P. Ding, and M. Jia, "Self-supervised pretraining via contrast learning for intelligent incipient fault detection of bearings," *Rel. Eng. Syst. Saf.*, vol. 218, Feb. 2022, Art. no. 108126.

[19] M. Xu, P. Baraldi, X. Lu, and E. Zio, "Generative adversarial networks with AdaBoost ensemble learning for anomaly detection in high-speed train automatic doors," *IEEE Trans. Intell. Transp. Syst.*, vol. 23, no. 12, pp. 23408–23421, Dec. 2022.

[20] J. Gilles, "Empirical wavelet transform," *IEEE Trans. Signal Process.*, vol. 61, no. 16, pp. 3999–4010, Aug. 2013.

[21] Y. Jiang, H. Zhu, and Z. Li, "A new compound faults detection method for rolling bearings based on empirical wavelet transform and chaotic oscillator," *Chaos, Solitons Fractals*, vol. 89, pp. 8–19, Aug. 2016.

[22] W. Liu and W. Chen, "Recent advancements in empirical wavelet transform and its applications," *IEEE Access*, vol. 7, pp. 103770–103780, 2019.

[23] A. Francis and C. Muruganantham, "An adaptive denoising method using empirical wavelet transform," *Int. J. Comput. Appl.*, vol. 117, no. 21, pp. 18–20, May 2015.

[24] I. J. Goodfellow, J. Pouget-Abadie, M. Mirza, B. Xu, D. Warde-Farley, S. Ozair, A. Courville, and Y. Bengio, "Generative adversarial nets," in *Proc. 27th Int. Conf. Neural Inf. Process. Syst.*, vol. 2, Montreal, QC, Canada, 2014, pp. 2672–2680.

[25] M. Arjovsky, S. Chintala, and L. Bottou, "Wasserstein generative adversarial networks," in *Proc. 34th Int. Conf. Mach. Learn.*, vol. 70, Sydney, NSW, Australia, 2017, pp. 214–223.

[26] I. Gulrajani, F. Ahmed, M. Arjovsky, V. Dumoulin, and A. Courville, "Improved training of Wasserstein GANs," in *Proc. 31st Int. Conf. Neural Inf. Process. Syst.*, Long Beach, CA, USA, 2017, pp. 5769–5779.

[27] M. Mendes and S. Yiğit, "Comparison of ANOVA-fand ANOM tests with regard to type I error rate and test power," *J. Stat. Comput. Simul.*, vol. 83, no. 11, pp. 2093–2104, Nov. 2013.

[28] Z. Gao, F. Shi, B. Zhang, and Y. Su, "Defect type recognition analysis of convolutional neural network," *J. Appl. Acoust.*, vol. 41, no. 2, pp. 301–309, 2022.

[29] H. Zhu and T. Fang, "Compound fault diagnosis of rolling bearings with few-shot based on DCGAN-RepLKNet," *Meas. Sci. Technol.*, vol. 35, no. 6, Mar. 2024, Art. no. 066105.

[30] B. Hu, J. Liu, R. Zhao, Y. Xu, and T. Huo, "A new dual-channel convolutional neural network and its application in rolling bearing fault diagnosis," *Meas. Sci. Technol.*, vol. 35, no. 9, Jun.27, 2024, Art. no. 096130.

[31] G. Fu, Q. Wei, and Y. Yang, "Bearing fault diagnosis with parallel CNN and LSTM," *Math. Biosciences Eng.*, vol. 21, no. 2, pp. 2385–2406, 2024.

[32] C. Zhou, Q. Wang, Y. Xiao, W. Xiao, and Y. Shu, "Research on an improved auxiliary classifier Wasserstein generative adversarial network with gradient penalty fault diagnosis method for tilting pad bearing of rotating equipment," *Lubricants*, vol. 11, no. 10, p. 423, Oct. 2023.

[33] Y. Lei, T. Han, B. Wang, N. Li, T. Yan, and J. Yang, "Interpretation of XJTU-SY rolling bearing accelerated life test dataset," *Chin. J. Mech. Eng.*, vol. 55, no. 16, pp. 1–6, 2019.

CHUNLEI ZHOU received the B.S. degree in process equipment and control engineering and the M.S. degree in power engineering and engineering thermophysics from Beijing University of Chemical Technology, Beijing, China, in 2021 and 2024, respectively. He is currently pursuing the Ph.D. degree in mechanical engineering with the University of Science and Technology Beijing.

His current research interests include deep learning and rotating machinery fault diagnosis.

WANG XIAO received the Ph.D. degree from the School of Mechanical Engineering, Xinjiang University, China.

He is currently a Senior Engineer with the Western Branch of National Pipe Network Group United Pipeline Company Ltd., China. His research interests include compressor fault diagnosis and prediction and health management.

QINGFENG WANG (Member, IEEE) received the Ph.D. degree from the College of Mechanical and Electrical Engineering, Beijing University of Chemical Technology, China, in 2011.

He is currently a Professor with the College of Mechanical and Electrical Engineering, Beijing University of Chemical Technology. He is also a Security Expert with the State Administration of Work Safety of China. His research interests include dynamic monitoring and maintenance, prediction and health management, and reliability engineering.

ZHIPENG FENG (Member, IEEE) received the B.S. degree in automotive engineering from Jilin University, Changchun, China, in 1997, the M.S. degree in mechanical engineering from Kunming University of Science and Technology, Kunming, China, in 2000, and the Ph.D. degree in power machinery engineering from Dalian University of Technology, Dalian, China, in 2003.

From 2003 to 2005, he was a Postdoctoral Fellow with the Department of Precision Instruments and Mechanology, Tsinghua University, Beijing, China. From 2006 to 2007, he was a Postdoctoral Research Fellow with the Department of Mechanical Engineering, University of Alberta, Edmonton, AB, Canada. He is currently a Professor with the School of Mechanical Engineering, University of Science and Technology Beijing, Beijing. His research interests include machinery fault diagnosis, signal processing, artificial intelligence, and mechanical dynamics.